Global Change Biology (2006) **12,** 1842–1867, doi: 10.1111/j.1365-2486.2006.01200.x

Modeling dynamics of stable carbon isotopic exchange between a boreal forest ecosystem and the atmosphere

BAOZHANG CHEN*, JING M. CHEN*, LIN HUANG† and PIETER P. TANS‡
*Department of Geography and Program in Planning, University of Toronto, 100 St. George Street, Room 5047, Toronto, ON, Canada M5S 3G3, †Atmospheric Science and Technology Directorate, EC, 4905 Dufferin Street, Toronto, ON, Canada M3H 5T4, ‡NOAA/ESRL's Global Monitoring Division, 325 Broadway R/CMDL1 Boulder, CO 80305, USA

Abstract

Stable isotopes of CO_2 contain unique information on the biological and physical processes that exchange CO_2 between terrestrial ecosystems and the atmosphere. In this study, we developed an integrated modeling system to simulate dynamics of stable carbon isotope of CO_2, as well as moisture, energy, and momentum, between a boreal forest ecosystem and the atmosphere, as well as their transport/mixing processes through the convective boundary layer (CBL), using remotely sensed surface parameters to characterize the surface heterogeneity. It has the following characteristics: (i) it accounts for the influences of the CBL turbulent mixing and entrainment of the air aloft; (ii) it scales individual leaf-level photosynthetic discrimination up to the whole canopy (Δ_{canopy}) through the separation of sunlit and shaded leaf groups; (iii) it has the capacity to examine the detailed interrelationships among plant water-use efficiency, isotope discrimination, and vapor pressure deficit; and (iv) it has the potential to investigate how an ecosystem discriminates against ^{13}C at various time and spatial scales. The monthly mean isotopic signatures of ecosystem respiration (i.e. $\delta^{13}C_R$) used for isotope flux calculation are retrieved from the nighttime flask data from the intensive campaigns (1998–2000) at 20 m level on Fraserdale tower, and the data from the growing season in 1999 are used for model validation. Both the simulated CO_2 mixing ratio and $\delta^{13}C$ of CO_2 at the 20 m level agreed with the measurements well in different phases of the growing season. On a diurnal basis, the greatest photosynthetic discrimination at canopy level (i.e. Δ_{canopy}) occurred early morning and late afternoon with a varying range of 10–26‰. The diurnal variability of Δ_{canopy} was also associated with the phases of growing season and meteorological variables. The annual mean Δ_{canopy} in 1999 was computed to be 19.58‰. The monthly averages of Δ_{canopy} varied between 18.55‰ and 20.84‰ with a seasonal peak during the middle growing season. Because of the strong opposing influences of respired and photosynthetic fluxes on forest air (both CO_2 and $^{13}CO_2$) on both the diurnal and seasonal time scales, CO_2 was consistently enriched with the heavier ^{13}C isotope (less negative $\delta^{13}C$) from July to October and depleted during the remaining months, whereas on a diurnal basis, CO_2 was enriched with the heavier ^{13}C in the late afternoon and depleted in early morning. For the year 1999, the model results reveal that the boreal ecosystem in the vicinity of Fraserdale tower was a small sink with net uptake of 29.07 g ^{12}C m^{-2} yr^{-1} and 0.34 g ^{13}C m^{-2} yr^{-1}.

Keywords: atmosphere, boreal ecosystems, carbon isotope, convective boundary layer, diffusion processes, discrimination, Fraserdale tower, isotope model, net ecosystem exchange, remote sensing

Received 18 October 2005; revised version received 3 March 2006; accepted 10 March 2006

Introduction

The global budget of atmospheric CO_2 is one of the crucial issues for prognoses of future climate change. Of the CO_2 emitted into the atmosphere resulting from fossil fuel consumption, roughly half remains in the

Correspondence: Baozhang Chen, tel. + 1416 978-7085, fax + 1416 946-3886, e-mail: chenb@geog.utoronto.ca

atmosphere whereas the rest is absorbed by the oceans and the terrestrial biosphere (Keeling *et al*., 1989; Tans *et al*., 1993). The partitioning between these two sinks is a subject of considerable debate. Whereas most terrestrial ecologists doubt that the land biosphere can be a large carbon sink, chemical oceanographers are confident that the oceanic sink is not large enough to account for the entire absorption and thus the issue of the 'missing' carbon sink arises (Ciais *et al*., 1995a). Stable isotopes of carbon dioxide in the atmosphere contain unique information to study the overall balance of surface CO_2 fluxes (Tans *et al*., 1990, 1993). Distinct isotopic signatures between oceanic and terrestrial discriminations (oceans discriminate roughly 10 times less against ^{13}C than most terrestrial plants) allow the isotopic signal in atmospheric CO_2 to be a powerful tracer for partitioning terrestrial and oceanic sinks of atmospheric CO_2 at the global scale (Keeling *et al*., 1989, 2001; Tans *et al*., 1993; Ciais *et al*., 1995b, 1999; Enting *et al*., 1995; Francey *et al*., 1995; Fung *et al*., 1997; Rayner *et al*., 1999; Battle *et al*., 2000).

Terrestrial ecosystems, as a major component of the climate system, involve several physical and physiological processes acting at different scales through the exchange of energy, momentum, and trace gases with the atmosphere; consequently, the spatial and temporal variations of these exchanges are difficult to assess. The existing and potential feedbacks between terrestrial ecosystem and atmosphere remain one of the largest uncertainties in our understanding of the global carbon cycle. The information on the biological and physical processes that exchange CO_2 between terrestrial ecosystems and the atmosphere is recorded by the signals of $^{13}C/^{12}C$ ratio in the atmosphere CO_2. As reviewed by Suits *et al*. (2005), carbon isotopes can be helpful in investigations of the following four aspects at ecosystem and local scales: (1) plant water-use efficiency and the response of plants to changes in precipitation and relative humidity (Farquhar & Richards, 1984; Farquhar *et al*., 1988; Condon *et al*., 1993; Hall *et al*., 1993; Schulze *et al*., 1996, 1998; Ekblad & Högberg, 2001; Bowling *et al*., 2002), (2) variation in light distribution and stand structure (Berry *et al*., 1997; Buchmann *et al*., 1997a, b; Le Roux *et al*., 2001), (3) recycling of respired CO_2 (Keeling, 1961; Schleser & Jayasekera, 1985; Sternberg, 1989; Lloyd *et al*., 1996; Sternberg *et al*., 1997), and (4) determining the relative contributions of photosynthesis and respiration to the total net ecosystem exchange (NEE; Yakir & Wang, 1996; Bowling *et al*., 2001; Lai *et al*., 2003; Ogée *et al*., 2003a; Knohl & Buchmann, 2005).

However, most existing approaches are dependent, to some degree, on measurements of $^{13}C/^{12}C$ in the atmosphere. Multiple efforts to measure carbon isotopes at both flux towers and flask stations around the world have been achieved. Several new techniques (e.g. automated measurement systems, tunable diode laser (TDL) spectrometer and pulsed quantum cascade laser spectrometer) have also been applied to this investigation (e.g. Bowling *et al*., 2003b; Lai *et al*., 2003, 2004; Griffis *et al*., 2004; Schauer *et al*., 2005; McManus *et al*., 2005). Available isotopic datasets have been accumulating quickly these years (e.g. Griffis *et al*., 2005; Lai *et al*., 2005a, b, 2006; Ponton *et al*., 2006), isotope measurements, however, are still lacking considering the land surface diversity/heterogeneity. This shortage of long-term measurements and of sampling frequency still limits isotopic studies and applications to various spatial/temporal scales.

Mechanistic biophysical models that couple micrometeorological and eco-physiological theories have the potential to shed light on how to extend efforts and applications of stable isotopes of carbon dioxide to global carbon budgeting, because biophysical models have the capacities of simulating isotope discrimination in response to environmental perturbations and can produce information on its diurnal, seasonal and interannual dynamics. Few biophysical models, however, have been developed to assess stable carbon discrimination between a plant canopy and the atmosphere (e.g. Baldocchi & Bowling, 2003; Ogée *et al*., 2003a; Suits *et al*., 2005). Most existing biophysical models are based on individual leaf level discrimination equations given by Farquhar *et al*. (1982, 1989) and only focus on the land surface layer (ignoring vertical and horizontal advection effects beyond 50–100 m above the ground, e.g. Baldocchi & Bowling, 2003). However, in nature, the convective boundary layer (CBL) integrates the effects of photosynthesis, respiration, and turbulent transport of CO_2 over the landscape (Lloyd *et al*., 1996; Pataki *et al*., 2003). The influence of the CBL cannot be ignored when using isotope composition of CO_2 to investigate biological processes (Bowling *et al*., 1999) because the effect of atmospheric stability on turbulent mixing/diffusion has an important impact on scalar fluxes and concentration fields within and above canopies (Baldocchi & Harley, 1995; Leuning, 2000). Few such models considering the CBL effects on isotope fractionation have been developed to the date (e.g. a model developed by Lloyd *et al*. (1996, 2001), which is dependent on campaign measurements and is limited to the short campaign periods).

In this study, we developed an integrated modeling system to simulate dynamics of stable carbon isotope of CO_2, moistures, energy, and momentum between a boreal forest ecosystem and the atmosphere, as well as their transport/mixing processes through the whole CBL. This system consists of two components: the vertical diffusion scheme (VDS) model (Chen *et al*.,

2004a) and an ecosystem model referred to as boreal ecosystem productivity simulator (BEPS2.0, which is a newer version that includes a land surface scheme, namely 'ecosystem–atmosphere simulation scheme' (i.e. EASS; Chen *et al*., 2006a, b). These two components are expanded to simulate $^{13}CO_2$ transport/mixing processes from the surface layer through the top of CBL as well as flux densities of $^{13}CO_2$ at the canopy level, which can be used to address many of the issues related to the dynamic exchange in stable carbon isotopes of CO_2 between terrestrial ecosystems and the atmosphere through the CBL and their responses to environment changes. First, the integrated VDS-BEPS2.0 isotope model system accounts for the influence of the CBL turbulent mixing and entrainment of the air aloft (Chen *et al*., 2004a), and therefore, many aspects of the temporal and spatial variations of the $^{13}CO_2$ concentration field can be reasonably simulated. Second, its 'two-leaves' model (with separation of sunlit and shaded leaves) enables it to scale leaf-level photosynthetic discrimination (Farquhar *et al*., 1982, 1989) up to the whole canopy in a computationally efficient and a practical way, with the expected characteristics of higher accuracy than simple 'big-leaf' model (Lloyd *et al*., 1996; Bowling *et al*., 2001). This modeling strategy can also be easily implemented in regional scale general circulation models (GCMs) compared with the 'multilayer' approach (Baldocchi & Bowling, 2003; Ogée *et al*., 2003a). Third, by coupling energy, water, photosynthesis, and stomatal conductance, the VDS-BEPS2.0 isotope model has the capacity of examining interrelationships between plant water-use efficiency, isotope discrimination, and vapor pressure deficits (VPD) with mechanistic details. Fourth, it does not rely on campaign measurements as model's boundary conditions because of its capability in simulating the CBL processes. It requires, however, the information on the carbon isotopic signatures of the atmospheric background (i.e. its values of the troposphere) and of respired CO_2 from the biosphere. And finally, by incorporating information from frequently updated satellite data which follows the seasonal variation in leaf area index (LAI) determining the photosynthetic capacity, the VDS-BEPS2.0 isotope model has the potential to investigate how a forest canopy discriminates against ^{13}C at different temporal scales (i.e. daily, seasonal, yearly, and interannual) and at large spatial scales (i.e. landscape or regional scale).

Now to an over view of the paper, the following section gives a brief review of the theoretical background of the basis of mass conservation. Next we follow this up with a section on the methodology used and outline of the VDS-BEPS2.0 isotope model. The detailed expansions in BEPS2.0 and in VDS for isotope simulations are described in Appendices. Model results from experimental runs for a boreal site (Fraserdale, northern Ontario, Canada) in 1999 and model validation against intensive campaign data at the site are provided and discussed in the penultimate section. The last section summarizes and concludes.

Review of the theoretical background

Isotope mass conservation

On the basis of conservation of mass, the atmospheric concentration of a gas (denotes C, mixing ratio ($\mu mol\,mol^{-1}$)) at a reference height (observed values, i.e. in the land surface layer or an adjacent boundary layer) in an arbitrary atmospheric column near the surface reflects the combination of some background atmospheric concentration and different amounts of that gas added from sources in both the vertical and horizontal directions (C_{source}). The source term C_{source}, in nature, could be from diverse sites. For a reference height over a terrestrial ecosystem, C_{source} might mostly result from local biological activities (C_{bio}), but also from net horizontal advection (C_{adv}, the difference between in-coming CO_2 and out-going to the observed site by advection and transport). The land surface heterogeneities, biomass burning, and the fossil fuel combustion (C_{ff}) (Miller *et al*., 2003; Lai *et al*., 2004) may be the major contributors to C_{adv}. Generally, the conservation equation for a certain gas in the atmosphere can be expressed as

$$C_{obs} = C_{bg} + C_{bio} + C_{adv}, \quad (1)$$

where C_{obs} and C_{bg}, are, respectively, the observed atmospheric CO_2 concentration at a reference site and the background value; C_{bio} and C_{adv} are the concentration components produced by local biological activities and by the net horizontal advection, respectively, which raise or reduce the atmospheric CO_2 concentration from the background value. In this paper, we focus on the atmospheric trace gas of CO_2, but the same arguments will apply to other gases, e.g., water vapor (e.g. Moreira *et al*., 1997) and methane (e.g. Thom *et al*., 1993). Multiplying each term in Eqn (1) by its isotope molar ratio ($R = {}^{13}C/({}^{12}C + {}^{13}C) \approx {}^{13}C/{}^{12}C$), we obtain an equation for isotope mass conservation

$$R_{obs}C_{obs} = R_{bg}C_{bg} + R_{bio}C_{bio} + R_{adv}C_{adv}. \quad (2)$$

We can convert this relationship to the common isotopic notation based on the standard definition of isotopic composition,

$$\delta_{sample} = ((R_{sample} - R_{standard})/R_{standard}). \quad (3)$$

Dividing Eqn (2) through by $R_{standard}$ and then adding with Eqn (1), we get the isotope conservative

equation in the common isotopic δ notation:

$$\delta^{13}C_{obs}C_{obs} = \delta^{13}C_{bg}C_{bg} + \delta^{13}C_{bio}C_{bio} + \delta^{13}C_{adv}C_{adv}. \quad (4)$$

Equation (4) illustrates once again that the product $\delta^{13}C \times C$ (in $\mu mol\,mol^{-1}$‰) is, to a very close approximation, conservative (Tans, 1980). Similar arguments apply to other isotope ratios such as $^{18}O/^{16}O$ and D/H (each application may have its own caveats) as well. The CO_2 mixing ratio and $\delta^{13}C$ measurements in terrestrial ecosystems are found to be dominated by biological activities during the growing season under the condition that the upwind ecosystems behave in a very uniform way (Bakwin *et al*., 1998; Potosnak *et al*., 1999), such that C_{adv} can be ignored since $C_{bio} \gg C_{adv}$ and $C_{obs} = C_{bg} + C_{bio}$. Rearranging Eqns (1) and (4), we obtain the following equation which effectively describes what happens during the growing season:

$$\delta^{13}C_{obs}C_{obs} = \delta^{13}C_{bio}C_{obs} + (\delta^{13}C_{bg} - \delta^{13}C_{bio})C_{bg}. \quad (5)$$

Equation (5) represents a two-end member mixing system under the condition of mass conservation, which was introduced by Tans (1980) and described by Miller & Tans (2003). It has the linear form: $Y = \alpha_1 X + \alpha_2$, and the slope ($\alpha_1$) is $\delta^{13}C_{bio}$. This is different from the form of regression first used by Keeling (1961), in which by plotting $\delta^{13}C$ vs. the reciprocal of the CO_2 concentration, the y-intercept is interpreted as the isotopic signature of the source or sink. In this study, the isotopic signal of ecosystem respiration (i.e. $\delta^{13}C_R$) can be retrieved using Eqn (5) applied to nighttime data, and the slope is $\delta^{13}C_R$.

Mass conservation of isotopic flux density

Conservation of mass has been used, as a fundamental, to describe the net exchange of CO_2 and $^{13}CO_2$ between ecosystems and the atmosphere (Lloyd *et al*., 1996, 2001; Yakir & Wang, 1996; Flanagan *et al*., 1996; Bowling *et al*., 2001, 2003a; Lai *et al*., 2003; Ogée *et al*., 2003b). The NEE of CO_2 at the interface between terrestrial ecosystems and the atmosphere is the result of carbon uptake during daytime by photosynthesis (gross primary production: F_A) and the carbon loss by respiration (total ecosystem respiration: F_R). F_R is a composite CO_2 release flux, comprising of autotrophic respiration (R_a, by foliage, stem, and roots) and heterotrophic respiration (R_h, by soil organisms). Thus NEE can be expressed as

$$NEE = F_A + F_R = F_A + R_a + R_h. \quad (6)$$

If F_A and F_R carry different CO_2 isotope signatures (it is often the case in nature), the total CO_2 mass balance and the isotopic ($^{13}CO_2$ or $CO^{18}O$) mass balance equations are not proportional. Using the notations recommended by Bowling *et al*. (2003a), we can express the isoflux ($F_{\delta 13}$ in $\mu mol\,m^{-2}\,s^{-1}$ ‰) as

$$\begin{aligned} F_{\delta 13} &= \delta^{13}C_{bio}\,NEE = \delta^{13}C_A F_A + \delta^{13}C_R F_R \\ &= (\delta^{13}C_a - \Delta_{canopy})F_A + \delta^{13}C_R^h R_h + \delta^{13}C_R^a R_a, \end{aligned} \quad (7)$$

where $\delta^{13}C_{bio}$, $\delta^{13}C_A$, $\delta^{13}C_R$, $\delta^{13}C_R^h$, and $\delta^{13}C_R^a$ are the flux-weighted stable carbon isotopic composition of net CO_2 flux, of gross primary production flux, of ecosystem respiration flux, of heterotrophic respiration flux, and of autotrophic respiration flux, respectively; $\delta^{13}C_a$ is the isotopic composition of ambient CO_2 in the canopy; and Δ_{canopy} is the whole-canopy integrated photosynthetic carbon isotope discrimination (for detail, see Appendix A). All terms in δ notation and Δ_{canopy} are in per mil (‰); F_A and F_R are in $\mu mol\,m^{-2}\,s^{-1}$. Monthly mean carbon isotopic signatures of heterotrophic respiration ($\overline{\delta^{13}C_R^h}$) and of autotrophic respiration ($\overline{\delta^{13}C_R^a}$) are shown in Fig. 1. $\overline{\delta^{13}C_R^h}$ was interpolated on the basis of discrete values calculated from all the nighttime data in the campaigns (1998–2000) using Eqn (5), while $\overline{\delta^{13}C_R^a}$ was obtained from model test runs (for detail see Appendix A).

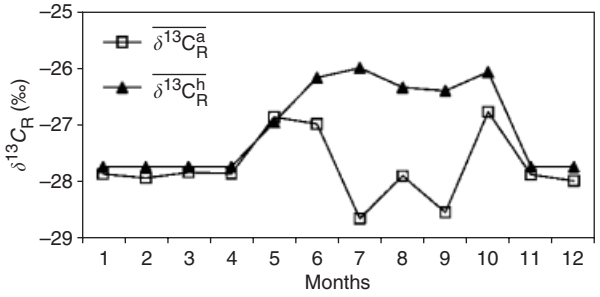

Fig. 1 Monthly mean carbon isotopic signatures of heterotrophic respiration ($\overline{\delta^{13}C_R^h}$) and of autotrophic respiration ($\overline{\delta^{13}C_R^a}$). $\overline{\delta^{13}C_R^h}$ was interpolated on the basis of the discrete values calculated from all the nighttime data in the campaigns (1998–2000) using Eqn (5), whereas $\overline{\delta^{13}C_R^a}$ was gained from model test run.

Methodology

Methodological strategy

In order to account for the influences of the CBL turbulent mixing and entrainment of the air aloft on diffusion and on the estimates of $^{13}CO_2$ discrimination, we designed a one-dimensional (1-D) VDS model for $^{13}CO_2$ based on conservation of mass and energy, which involves the interaction between plant canopies and the atmosphere in the surface layer (i.e. ^{13}C dis-

crimination) and $^{13}CO_2$ diffusion within the mixed layer.

We can expand our knowledge on isotopic conservation of mass at the surface layer to the whole planetary boundary layer (PBL) by taking a column of air extending from the canopy height (or the land surface layer) up to the top of the PBL. If we denote the total mass of the air column in PBL as M for fair weather conditions during daytime and the fraction of exchanged mass caused by uplifting plumes from the lower surface layer per unit time as dM_1/dt, and the fraction of exchanged mass caused by entraining from the top of the PBL per unit time as dM_2/dt, neglecting net horizontal advection of CO_2 and taking the product of $\delta^{13}C$ multiplying CO_2 mixing ratio to be conservative rather than $\delta^{13}C$, the following equation for the carbon isotope can be formulated from the following mass conservative equation:

$$M\frac{\partial(\delta^{13}C_mC_m)}{\partial t} = \frac{dM_1}{dt}\left(\delta^{13}C_sC_s - \delta^{13}C_mC_m\right) + \frac{dM_2}{dt}(\delta^{13}C_tC_t - \delta^{13}C_mC_m), \quad (8)$$

where C_s, C_m, and C_t are the CO_2 mole fraction of air in the lower surface layer, in the mixed layer, and at the top of the PBL, respectively, all in $\mu mol\,mol^{-1}$, and $\delta^{13}C$ represents its $^{13}CO_2$ component in δ notation, respectively, corresponding to C_s, C_m, and C_t. Combining equations for virtual potential temperature within the CBL on the basis of energy conservation (Chen *et al*., 2004a, 2005), we can obtain a solution for Eqn (8) (see Appendix B).

Outline of the VDS-BEPS 2.0 isotope model

An integrated modeling system (Chen *et al*., 2004a), which consists of two coupled components (VDS and BEPS2.0), is extended to have the capacity of simulating dynamics of stable carbon isotope through the whole CBL. BEPS2.0 was expanded to include a submodel to simulate photosynthetic discrimination and net isotope flux at canopy level (for detail see Appendix A); whereas VDS was expanded to simulate diffusion/mixing processes of stable carbon isotope of CO_2 from the surface layer through the top of the CBL (for details see Appendix B).

VDS-BEPS2.0 has been updated since Chen *et al*. (2004a). A new module for simulating the stable boundary layer (SBL) is introduced in the new version. The lower surface layer in this model is set at a fixed height of 20 m. The levels above are separated into intervals of 50 m in the model domain (2520 m, see Fig. 2 in Chen *et al*., 2004a). Totally, 51 layers are considered and the time step is 30 s. There are different schemes to treat different situations of the PBL structures (SBL or CBL) (Chen *et al*., 2005). The criteria that determine which module is applicable are the sign and magnitude of the bulk Richardson number (R_b) in the surface layer, and the magnitude of the ratio of the CBL height to the Monin Obukhov length ($|z_h/L|$).

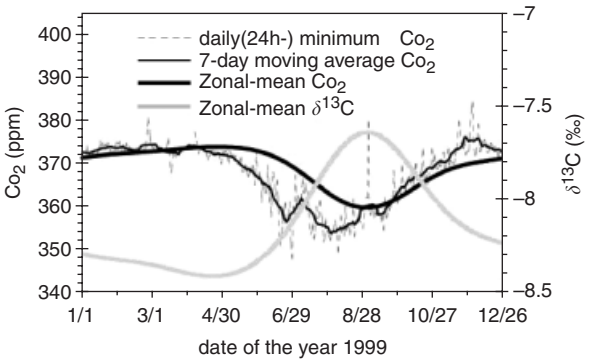

Fig. 2 Comparison of tower-observed daily minimum CO_2 mixing ratios at 20 m height and 7-day moving averages at Fraserdale, with zonal-mean CO_2 mixing ratio in marine boundary layer at the latitude corresponding to this site.

Model boundary conditions

Bottom boundary conditions for VDS. The model bottom conditions are the fluxes of sensible heat, carbon and isotopic $^{13}CO_2$ in the surface layer (the bottom layer of the model domain, i.e. 20 m height). We assume that the air storages of heat, carbon and carbon isotope between the plant canopy height (=10–15 m) and the lower surface layer of the model domain (20 m high above the ground) are negligible. We take the simulated fluxes at the plant canopy height and values at the bottom of model domain to be approximately equal. These three fluxes at the plant canopy height, i.e. sensible heat flux (Q_h), net CO_2 flux (NEE) and net isotopic flux ($F_{\delta 13}$), are modeled from the expanded BEPS2.0 isotope model (see Appendix A).

Top boundary conditions for VDS. The sensible heat flux above 2.5 km from the ground ($Q_{h,50}$, usually above CBL) is set to zero throughout the year. However, as 1-D model boundary condition, it is critical to determine the time-dependent CO_2 and $\delta^{13}C$ of CO_2 at the top of CBL. The technique making use of both the 24 h minima tower measurements and the Globalview reference marine boundary layer (MBL) matrix data (Chen *et al*., 2004a) is introduced for CO_2 top condition calculation, whereas MBL-$\delta^{13}C$ data are approximately used as its top condition since the $\delta^{13}C$ values

corresponding to the 24 h minima tower measurements are not available.

The Globalview reference MBL matrix from NOAA/CMDL's network is constructed in weekly intervals with spatial increment of 0.05 sine of latitude by using observations from sampling sites located in the marine boundary layer (Conway *et al*., 1994; Francey *et al*., 1995; Trolier *et al*., 1996), isolated from biospheric carbon sources and sinks (Masarie & Tans, 1995; Globalview-CO_2, 2005). Methodologies and procedures for constructing the Globalview reference MBL-CO_2 matrix are documented by Globalview-CO_2 (2005) and Masarie & Tans (1995), and are available on the internet via anonymous FTP to ftp://ftp.cmdl.noaa.gov/ccg/co2/GLOBALVIEW/. The Globalview reference MBL-$\delta^{13}CO_2$ matrix is specifically constructed using similar methods for the MBL-CO_2 matrix. These matrix data facilitate our model to be applicable to any continental sites over the world and to be coupled to global circulation models as well. For a particular site, one can use a linear interpolation method to extract MBL values of CO_2 mixing ratio and $\delta^{13}C$ between two nearest latitudes in the Globalview reference MBL-CO_2 and MBL-$\delta^{13}C$ matrices (Masarie & Tans, 1995; Globalview-CO_2, 2005). The MBL values of the CO_2 mixing ratio and $\delta^{13}C$ corresponding to the Fraserdale site, as well as the 24 h minima tower measurements of CO_2, are shown in Fig. 2.

Model input data

The BEPS2.0 (i.e. BEPS-EASS) isotope model is forced by the near-surface meteorological variables (i.e. at 20 m height in this study), including air temperature (T_a), air relative humidity (RH), in-coming short-wave radiation (RAD), wind speed (u), and precipitation (P). The land surface data, including vegetation and soil data, are also needed as model inputs. Most of the time-varying vegetation parameters, such as land cover, LAI, etc., are derived from satellite images (Cihlar *et al*., 1999; Chen *et al*., 2002). Data on soil texture (silt and clay fraction) and carbon pools are obtained from the Soil Landscapes of Canada (SLC) database version 1.0 and 2.0 (Shields *et al*., 1991; Schut *et al*., 1994; Lacelle, 1998).

Experiment site characteristics and measurements

The Fraserdale tower is located southwest of James Bay in northern Ontario, Canada (49°52′29.9″N, 81°34′12.3″W; 210 m above sea level). According to a Landsat TM image at a 30 m resolution (2000), the landscape (3600 km^2 around the tower) consists of 66% of black spruce (*Picea mariana*) and Jack pine (*Pinus banksiana*), 20% open land after forest fires and logging, 11% aspen (*Populus tremuloides*) and paper birch (*Betula papyrifera*), and 3% open water. The over-story vegetation heights around this site are ranging from 10 to 15 m.

The atmospheric CO_2 mixing ratio is continuously monitored at 40 and 20 m heights at the Fraserdale tower. The measurements are made according to the WMO (Global Atmospheric Watch) guidelines, with an accuracy of 0.1 ppm (Higuchi *et al*., 2003). T_a, RH, u, and RAD are also measured. For detailed site descriptions and CO_2 measurements, see Higuchi *et al*. (2003) and Chen *et al*. (2005).

Eight intensive campaigns for flask-air sampling were conducted in different seasons during the period 1998–2000 at this site. Each campaign lasted 3–6 days, with a sampling frequency of 2 h. Air samples were taken in 2 L flasks at the 20 m level of the tower. The flasks were pressurized up to 15 PSI above ambient pressure and were dried cryogenically (−70 °C) to remove water vapor. Almost all the samples from the campaigns were analyzed within 2 months. CO_2 from each 2 L sample was extracted cryogenically in a vacuum system and this was followed by isotopic ratio mass spectrometer (IRMS) analysis (MAT252, Finnigan, Germany). The isotopic measurements were directly traced back to the primary standard VPDB through two-carbonate linkages (i.e. lab running standards) (Huang *et al*., 2003). The assigned ratio for the primary standard (VPDB CO_2) is 0.0112372 for carbon (Allison *et al*., 1995). The accuracy and precision (including vacuum extraction and IRMS measurements) is 0.02‰ for $\delta^{13}C$ (Huang *et al*., 2003).

All the nighttime data in the campaigns (1998–2000) at the Fraserdale site were used for deriving the isotopic composition of ecosystem respiration (i.e. $\delta^{13}C_R$) by Eqn (5). The estimated $\delta^{13}C_R$ varies seasonally within a range from -24.958 ± 1.162‰ to -27.730 ± 1.002‰ (Table 1).

Results and discussions

Model validation

This integrated model system has been validated for several sites against campaigns and eddy measurements, such as Fluxnet Canada's towers measurements and concentration tower measurements (i.e. Fraserdale, Canada), as well as high tower measurements (i.e. the WLEF tower, see Chen *et al*., 2006d). It is known to perform well across different ecosystems in simulating the land surface fluxes of carbon, water and energy (Liu *et al*., 1997, 1999, 2002; Matsushita & Tamura, 2002; Wang *et al*., 2003; Sun *et al*., 2004; Chen *et al*., 2006a, b) and in simulating plant/soil temperatures and soil moistures (Chen *et al*., 2006a, b).

Table 1 Estimated isotopic components of ecosystem respiration ($\delta^{13}C_R$) in a boreal ecosystem using Eqn (5) against the nighttime campaigns data, 1998–2000, Fraserdale, Ontario, Canada*

Date	1998, day: 271–276	1999, day: 153–158	1999, day: 202–204	1999, day: 253–255	2000, day: 105–108	2000, day: 160–163	2000, day: 207–210
$\delta^{13}C_R$	−24.958	−26.165	−25.997	−26.397	−27.730	−27.590	−26.339
SE	± 1.162	± 0.194	± 0.376	± 0.370	± 1.002	± 0.525	± 0.631
r^2	0.9706	0.9991	0.9993	0.9980	0.9758	0.9967	0.9960
n	16	16	10	12	21	11	9

*SE is the standard error for $\delta^{13}C_R$ estimation; r^2 is the squared linear regression coefficient; and n is the sample number.

In the previous studies, it has also been proved that the combined VDS-BEPS2.0 model can simulate closely the observed CO_2 concentration. It was validated against the measured hourly averaged CO_2 concentration at 40 m height for the 12-year record (1990–1996 and 1999–2003) at Fraserdale tower (the squared correlation coefficients $r^2 = 0.70$, the root mean square error RMSE = 5.67 ppm and the sample number $n = 95\,979$). For 10-day averaged hourly values, the agreement between measurements and the model is significantly improved ($r^2 = 0.83$, RMSE = 1.08 ppm, and $n = 10\,236$) because the effects of horizontal advection and infrequent vertical diffusion associated with synoptic events are damped. The root mean square differences expressed in percentage of the averaged observation values (RMSD) are lower than 2% across different time scales. This suggests that VDS has the capacity of capturing most variations in CO_2 mixing ratios at the surface layer (Chen *et al.*, 2005). Simulated vertical patterns of the CO_2 mixing ratio are also comparable with those measured on the North Carolina tower (Chen *et al.*, 2004b). To further verify model performance in simulating vertical diffusion processes, VDS has recently been applied to the WLEF tower (Chen *et al.*, 2006d). VDS is validated against observed CO_2 mixing ratios at the heights of 30, 122, and 396 m for 2001. The regression statistics show that the values of r^2 at hourly time steps equal 0.69, 0.79, and 0.83 for 30, 122, and 396 m, respectively. Correspondingly, RMSE values equal 3.63, 2.84, and 2.6 ppm for 30, 122, and 396 m, respectively. It is verified that it performs well in simulating CO_2 vertical diffusion processes (Chen *et al.*, 2004a, 2005).

The intensive campaigns data collected in 1999 (February 16–17, June 2–7, July 21–23, and September 10–12) were used for validating the model performance in $\delta^{13}C$ simulation in the surface layer. The modeled and measured results for these three periods in 1999 are compared and discussed as follows.

The early phase of the growing season, June 2–7, 1999. Measured and modeled hourly results of several environmental parameters in the surface layer during June 2–7, 1999 at the Fraserdale tower site are shown in Fig. 3. The measured RAD peaked at about 700–900 W m^{-2} under fair weather conditions (Fig. 3a). Correspondingly, the calculated daily maximum of the photosynthetic photon flux density (PPFD) ranged from 900 to 1400 μmol m^{-2} s^{-1} (Fig. 3c), and the diurnal peak of sensible heat flux (H) was from 150 to 200 W m^{-2}, and the maximum of the PBL height (z_i) reached 1500–1800 m (Fig. 3f). The simulated net radiation (R_n) followed the variation of RAD well. During daytime, about two-thirds of R_n was released as latent heat flux (LE), and the remaining energy was released mainly as H (Fig. 3a). It was rainy on June 2 with a total of 9.6 mm rainfall. T_a during the 5 days ranged from 0 °C to 30 °C with a maximum diurnal amplitude of 23 °C. The simulated hourly canopy temperature (T_{canopy}) was close to the measurements. T_{canopy} was higher than T_a at mid-day, but lower during nighttime (Fig. 3b). High evaporative demand was apparent most afternoons as vapor pressure defect (VPD) approached 1.5–2.5 kPa (Fig. 3d). Both of T_a and VPD had increasing trends during this week.

Simulated diurnal variations in CO_2 fluxes and isofluxes above the canopy are shown in Figs 4a and b. Modeled ecosystem respiration (F_R) was somewhat related to T_a, nearly constant at nighttime and increases from sunrise to mid-afternoon. Photosynthetic uptake quickly increased from sunrise to mid-morning and slowly decreased during the afternoon and ceased at about sunset. The decreasing rate was dependent on the degree of water stress. There was significant day-to-day variability in fluxes, but consistent diurnal patterns were modeled. The net CO_2 flux peaked on average at about 10 μmol m^{-2} s^{-1}. Comparing Fig. 4a with Figs 3b–d, one can find that photosynthesis was sensitive to T_a, PPFD, and VPD. Patterns for isofluxes were similar (Fig. 4b), with a mid-day peak of 380 μmol m^{-2} s^{-1} ‰.

Modeled CO_2 mixing ratio at 20 m height closely followed tower observations and campaign flask measurements (Fig. 4c). The model captured the diurnal variations of $\delta^{13}C$ in the surface layer well (Fig. 4d).

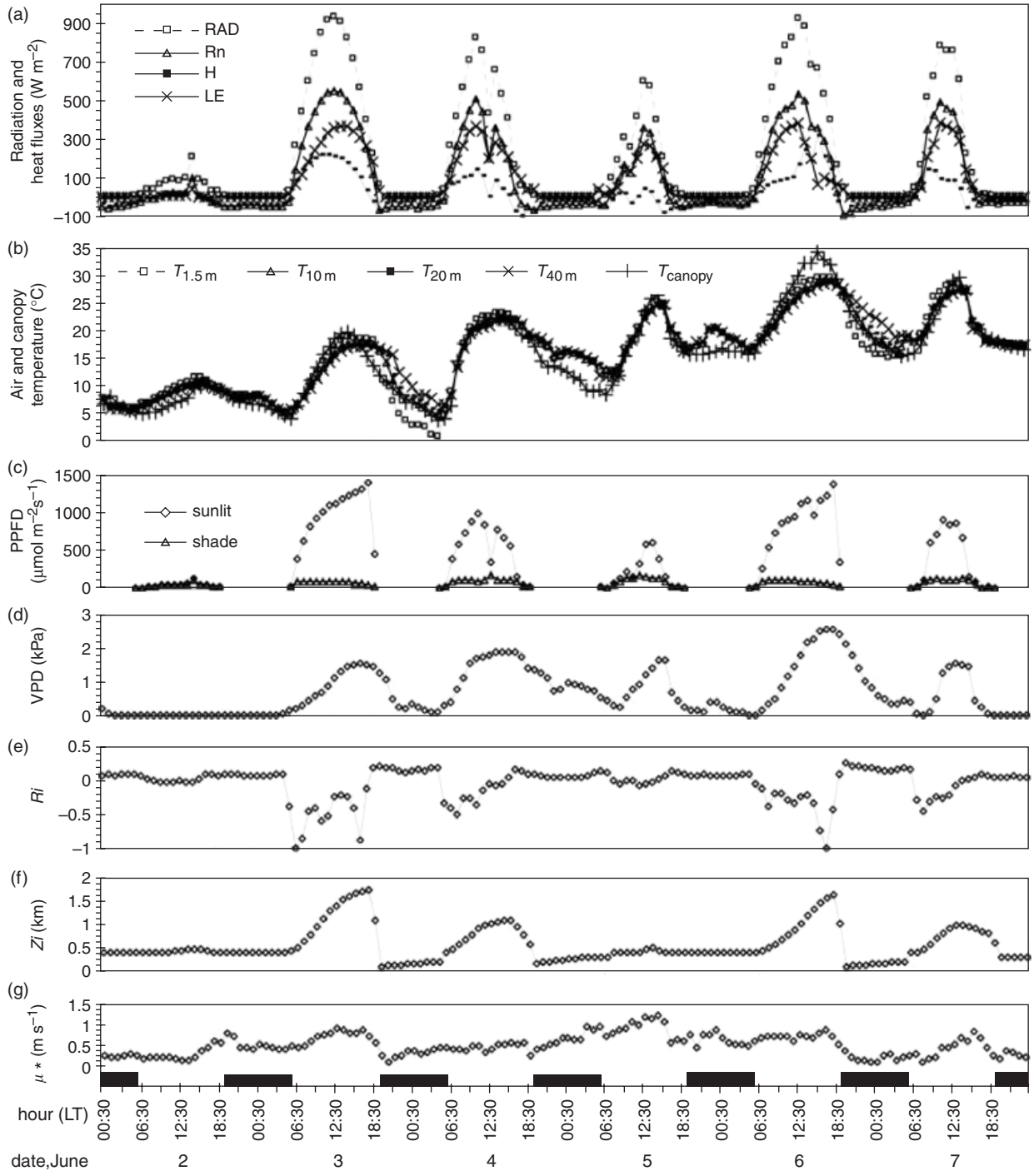

Fig. 3 Measured and modeled diurnal variations in several environmental parameters in the surface layer during June 2–7, 1999 at the Fraserdale tower site. (a) Measured total incoming solar radiation (RAD) and simulated net radiation (R_n), sensible heat flux (H), and latent heat flux (LE); (b) measured air temperature at the heights of 1.5 m ($T_{1.5\,m}$), 10 m ($T_{10\,m}$), 20 m ($T_{20\,m}$), 40 m ($T_{40\,m}$) above the ground and simulated vegetation canopy temperature (T_{canopy}); (c) simulated photosynthetic photon flux density (PPFD) on sunlit and shaded leaves; respectively; (d) measured vapor pressure deficit (VPD); (e) calculated gradient Richardon number (Ri) at the vegetation canopy height; (f) simulated planetary boundary layer (PBL) height (Zi); and (g) measured friction wind speed (μ_*). Dark bars on the horizontal axis in this and subsequent figures denote nocturnal periods.

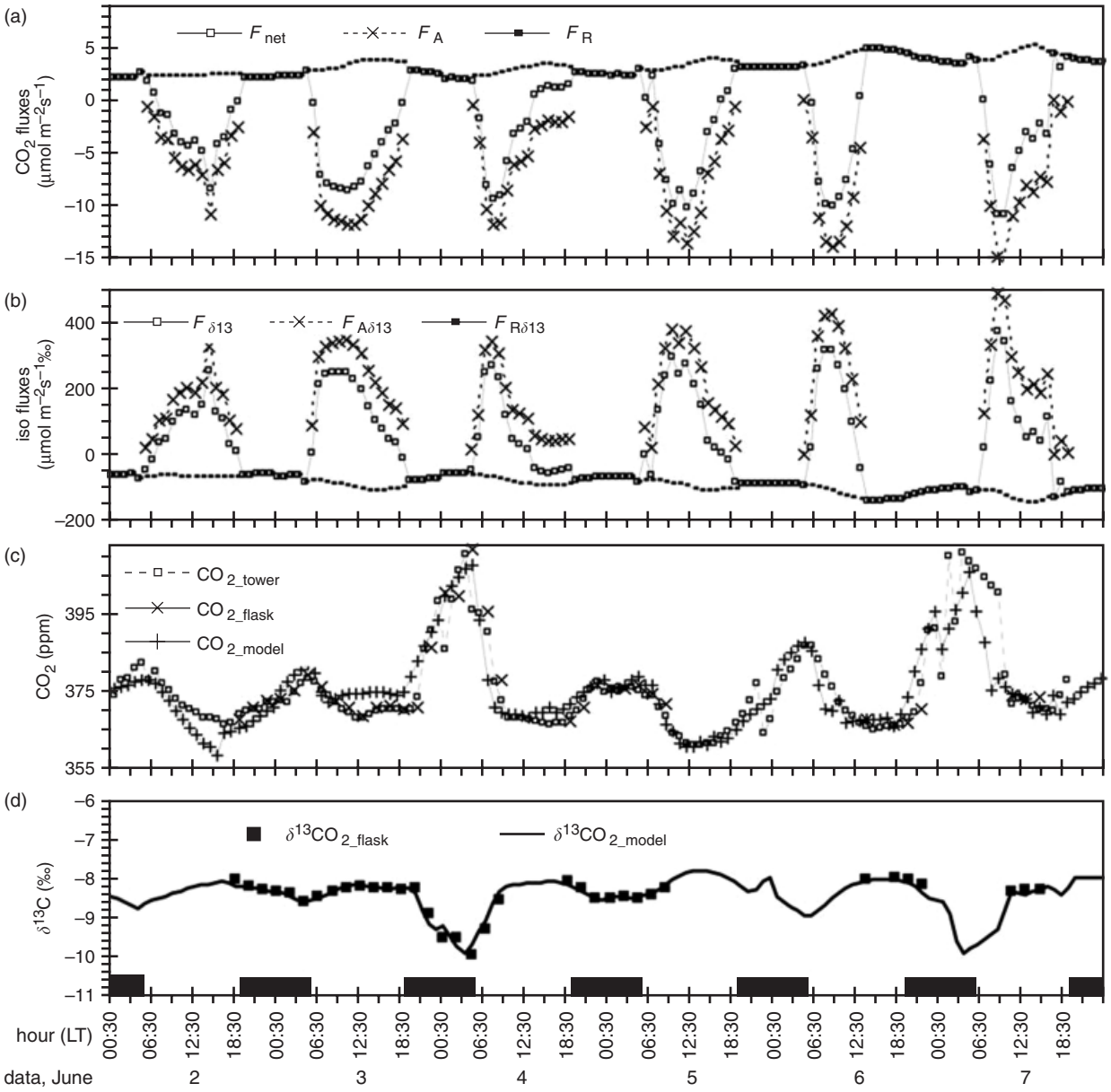

Fig. 4 Measured and modeled diurnal variations in net CO_2 flux and mixing ratio in the surface layer during June 2–7, 1999 at Fraserdale tower site. (a) Simulated CO_2 fluxes at the canopy height, which are net CO_2 flux (F_{net}), net assimilation (F_A), and total ecosystem respiration (F_R); (b) simulated isofluxes of $\delta^{13}C$ ($F_{\delta 13}$, $F_{A\delta 13}$, and $F_{R\delta 13}$) corresponding to F_{net}, F_A, and F_R, respectively; (c) simulated and observed CO_2 mixing ratios at 20 m height (which are: the observed hourly mean values (CO_{2_Tower}, which are the averages of original six discrete tower measurements with an accuracy of 0.1 ppmv; the range of the six data points within an hour is mostly less than 2 ppm), the intensive campaign data (CO_{2_flask}, which are flask sampled for around 5 min at each corresponding hour), and simulated hourly averaged data (CO_{2_model}); and (d) simulated and flask measured $\delta^{13}C$ of CO_2 at 20 m height.

The strong opposing influences of respiration and photosynthesis on forest air (both CO_2 concentration and its isotopic signature) were apparent (Figs 4c and d). CO_2 was consistently depleted with heavier ^{13}C isotope (more negative $\delta^{13}C$) in the early morning and enriched in the late afternoon (Fig. 4d). There was a more obvious day-to-day variability in both the CO_2 mixing ratio and $\delta^{13}C$ than that in net CO_2 and isotopic fluxes in the surface layer (comparing Figs 4c and d with Figs 4a and b). This may suggest that both the $\delta^{13}C$ and CO_2 concentrations in the surface layer were not only determined by their net fluxes but also by the atmosphere stability and mixing strength (these characteristics can be captured by our 1-D model) or this may reflect the significant difference in footprint areas between the fluxes and the $\delta^{13}C$ and CO_2 mixing

ratios (our 1-D model does not have the ability to simulate horizontal heterogeneity). At the nights preceding June 4 and June 7, for example, there existed a stable air condition with shallow nocturnal boundary layer (NBL: within 170 m, Fig. 3f), great air temperature inversion (Fig. 3b), high Richardson number *Ri* (about 0.15–0.20, Fig. 3e), and low friction velocity μ_* (Fig. 3g). Although the F_R and its isoflux ($F_{R\delta 13}$) at these two nights were small (Figs 4a and b), comparing with other nights, the built-up CO_2 reached high values (with maximum over 400 ppm, Fig. 4c) and $\delta^{13}C$ approached most negative values in this week due to accumulation of respired CO_2 with depleted ^{13}C in the surface layer when the vertical diffusion was suppressed by the inversion (the NBL was very shallow, Fig. 3f). $\delta^{13}C$ in the surface layer was mainly controlled by the respiratory isotopic flux and the NBL conditions during nighttime, while during the daytime, it was mostly determined by the photosynthetic isotopic flux, the isotopic signature of the preceding day's residual layer, and turbulent transport/mixing in the CBL, as well as entrainment from above the CBL. Comparisons between June 6 and 7 demonstrate some of these effects. Though the daytime net isofluxes on June 6 and on June 7 were similar, both the measured and modeled $\delta^{13}C$ at 20 m on June 6 were more positive than those on June 7 by about 0.3‰. Correspondingly, CO_2 mixing ratio on June 6 was lower than that on June 7 by about 4 ppm (Figs 4c and d). The main reason is possibly that stronger mixing/transport occurred on 6th than on 7th (CBL: 1.6 km vs. 1.0 km, Fig. 3f). The preceding night's $\delta^{13}C$ signature may also be another minor cause (there was more depleted heavier ^{13}C isotope on the night preceding 7th by around 1‰, Fig. 4d).

The middle phase of the growing season, July 21–23, 1999. There were cloudy conditions during this 3-day campaign. Measured and modeled hourly data of several environmental parameters in the surface layer during July 21–23, 1999 at the Fraserdale site are shown in Fig. 5. Except for air temperature, the magnitudes of most environmental parameters were similar to those in early growing season (comparing Fig. 5 with Fig. 3). The simulated CO_2 fluxes and isofluxes in the middle growing season were larger than those in the early growing season by around 10% (Figs 4 and 6). There was a small day-to-day variability in both the simulated and modeled $\delta^{13}C$ and CO_2 mixing ratios during these 3 days (Figs 6c and d) because of similar diurnal variations in environmental parameters.

The late phase of the growing season, September 10–12, 1999. This 3-day campaign was under cloudy-shower weather conditions. The daily total rainfall was 4.8, 2, and 5.4 mm, respectively. The RAD was comparatively low in this period and consequently PPFD, R_n, H, and LE were also low (Fig. 7). Diurnal amplitudes of most environmental parameters were small too. The air temperature during these 3 days ranged from 8 °C to 15 °C with a small diurnal amplitude (7 °C, Fig. 7b). Low evaporation made VPD below 0.6 kPa (Fig. 7d). The simulated maxima of CO_2 fluxes (F_{net} and F_A) and isofluxes ($F_{\delta 13}$ and F_{A13}) during these 3 days were slightly less than those in the early growing season though RAD was much lower because of the differences in VPD between these two campaign's periods (compare Fig. 7 with Fig. 3 and Fig. 8 with Fig. 4). Different weather conditions (mostly in VPD) also caused dissimilar diurnal patterns in CO_2 and carbon isotopic fluxes (compare Fig. 8 with Fig. 4). On clear days (i.e. June 2–7) the maximum photosynthesis rate lasted only 2–3 h (Fig. 4a) while under cloudy-shower weather conditions (i.e. September 10–12 and July 21–23) the maximum uptake remained for 5–6 h (Figs 6a and 8a). Modeled values of the CO_2 mixing ratio and $\delta^{13}C$ at 20 m height traced tower observations and campaign flask measurements well (Figs 8c and d). Both the modeled and observed diurnal variations in CO_2 and $\delta^{13}C$ during these three days were lower (Figs 8c and d) than with other two campaign periods (Figs 4c, d, 6c, and d) because of the differences in air stability (i.e. deeper NBL and shallower CBL, see Fig. 7f) and temperature inversion (Fig. 7b).

Modeled and tower measured hourly averaged CO_2 mixing ratios for the three campaign periods in 1999 are plotted in Fig. 9, whereas simulated hourly averaged $\delta^{13}C$ and campaign measured $\delta^{13}C$ are plotted in Fig. 10. The values of r^2 for both the CO_2 and $\delta^{13}C$ are above 0.7 for the three different phases of the growing season in 1999. Performance of the expanded VDS-BEPS2.0 isotope model, overall, was satisfactory in simulating the diurnal variation of CO_2 and $\delta^{13}C$ at 20 m height over the whole course of the growing season. However, our model trends to underestimate both the CO_2 and $\delta^{13}C$ (i.e. linear regression slop <1, Figs 9 and 10). The model underestimates the diurnal maximum of the CO_2 mixing ratio and overestimates the minimum of $\delta^{13}C$ (see Figs 4, 6, and 8–10). These model biases may result from ill parameterization of eddy-transfer coefficient K or overestimation of the height of the NBL in the model. The results of regression analyses between the simulated and measured hourly CO_2 mixing ratio and $\delta^{13}C$ in the surface layer for the three campaign periods in 1999 are list in Table 2. RMSE values were less than 5 ppm and 0.4‰ for CO_2 and $\delta^{13}C$, respectively, in different growing season phases in 1999. Correspondingly, RMSD values were lower than 5%. The diurnal

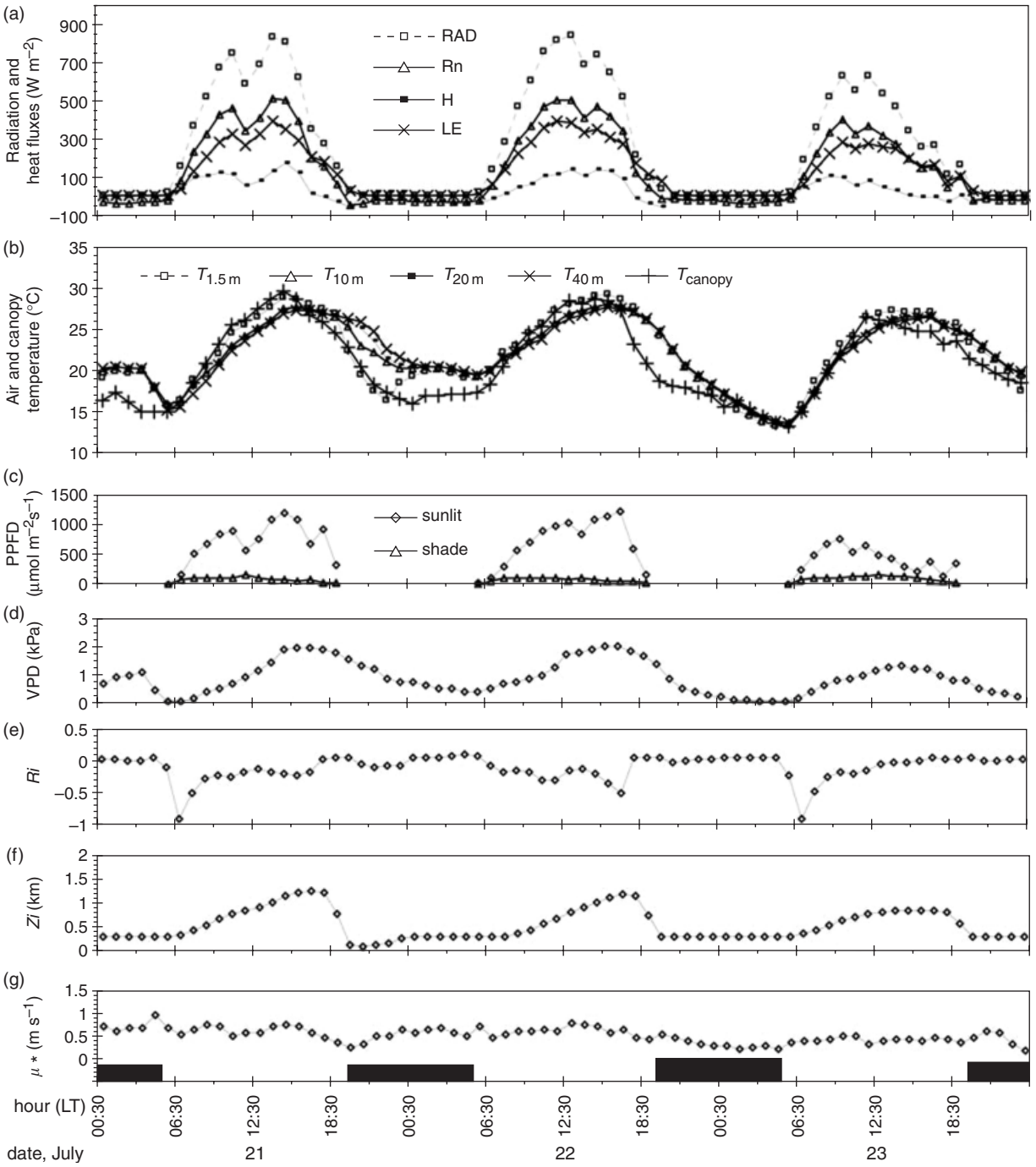

Fig. 5 Same as Fig. 3, but for July 21–23, 1999.

variations in both CO_2 and $\delta^{13}C$ were simulated well in the growing season.

Modeled canopy isotope discrimination (Δ_{canopy})

Measurements of photosynthetic discrimination at canopy level are time consuming and require special apparatus. Daily estimates of Δ_{canopy} over a corn–soybean rotation ecosystem in the Upper Midwest United States for a 192-day period during the corn (C4) phase of the 2003 growing season using a TDL and gradient technique were reported in Griffis *et al*. (2005). Seasonal averages of Δ_{canopy} in forest biomes across the United States were estimated based on flask data collected by an automated air sampling system (15 flasks weekly during the growing season) were documented in Lai

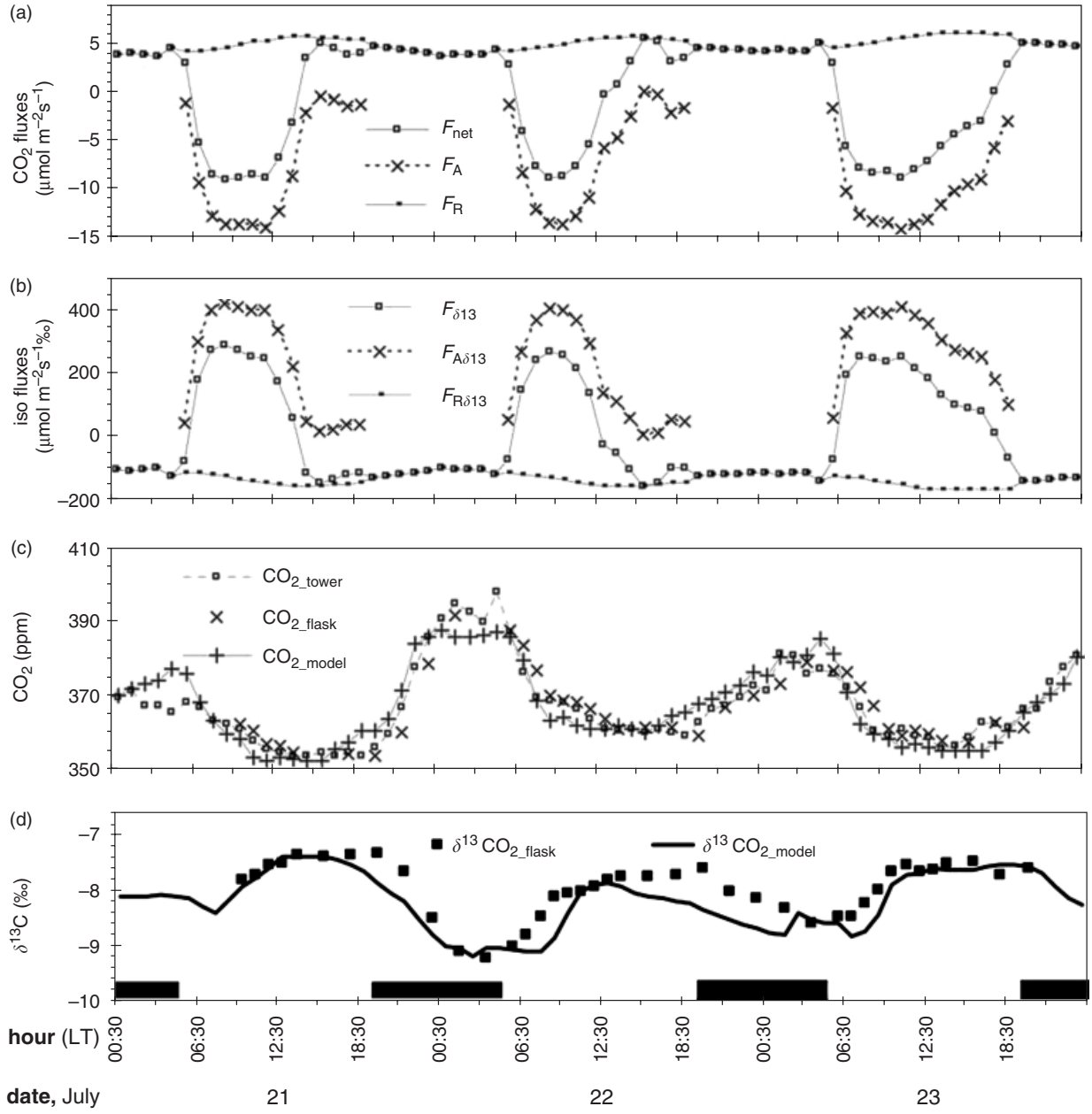

Fig. 6 Same as Fig. 4, but for July 21–23, 1999.

et al. (2005a, b). Long-term measurements of Δ_{canopy} are still lacking and no instantaneous estimates (e.g. hourly) of Δ_{canopy} are available in the literature for comparison. To provide insights on how Δ_{canopy} may change over the course of a growing season and respond to environmental perturbations, we present the model results in the following.

On a diurnal basis, the greatest differences occurred during the early morning and late afternoon and differences had a range of 10–26‰. Simulated diurnal variations in Δ_{canopy}, g_s, and A during the three campaign periods are shown in Figs 11–13. There were significant differences in the diurnal variability of Δ_{canopy} among the different phases of the growing season. Diurnal amplitudes of Δ_{canopy} found in the first campaign (i.e. the early phase of the growing season, June 2–7) were around 10‰, and these were larger than the values in the last campaign (i.e. the late phase of the growing season, September 10–12) which were about 1‰. Δ_{canopy} is proportional to the ratio of A to g_s (Eqn (A4)), and it is related also to several environmental factors. Diurnal variations in RAD, T_a, and VPD were more obvious

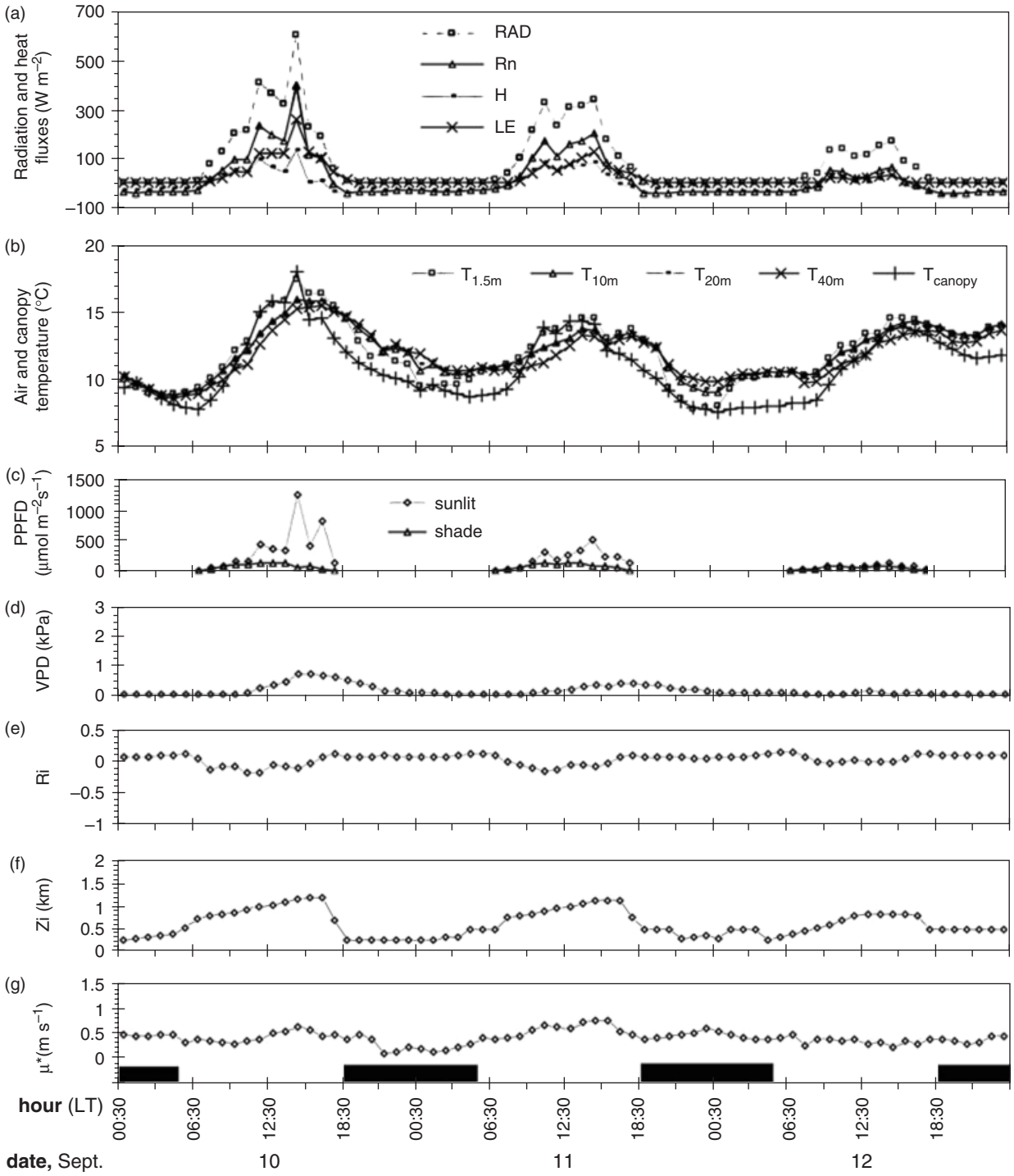

Fig. 7 Same as Fig. 3, but for September 10–12, 1999.

during the first campaign period than those during the last campaign period which was under cloudy-shower weather conditions (Figs 3, 5 and 7). This suggests that the diurnal patterns of Δ_{canopy} varies in the growing season and are associated with environmental variables.

These diurnal patterns of Δ_{canopy} are similar to those simulated for a temperate broad-leaved forest ecosystem near Oak Ridge, Tennessee (latitude 35°57′30″N; longitude 84°17′15″W) in 1998 (Baldocchi and Bowling, 2003). Greatest Δ_{canopy} values occur near sunrise and sunset, when photosynthesis rates diminish relative to

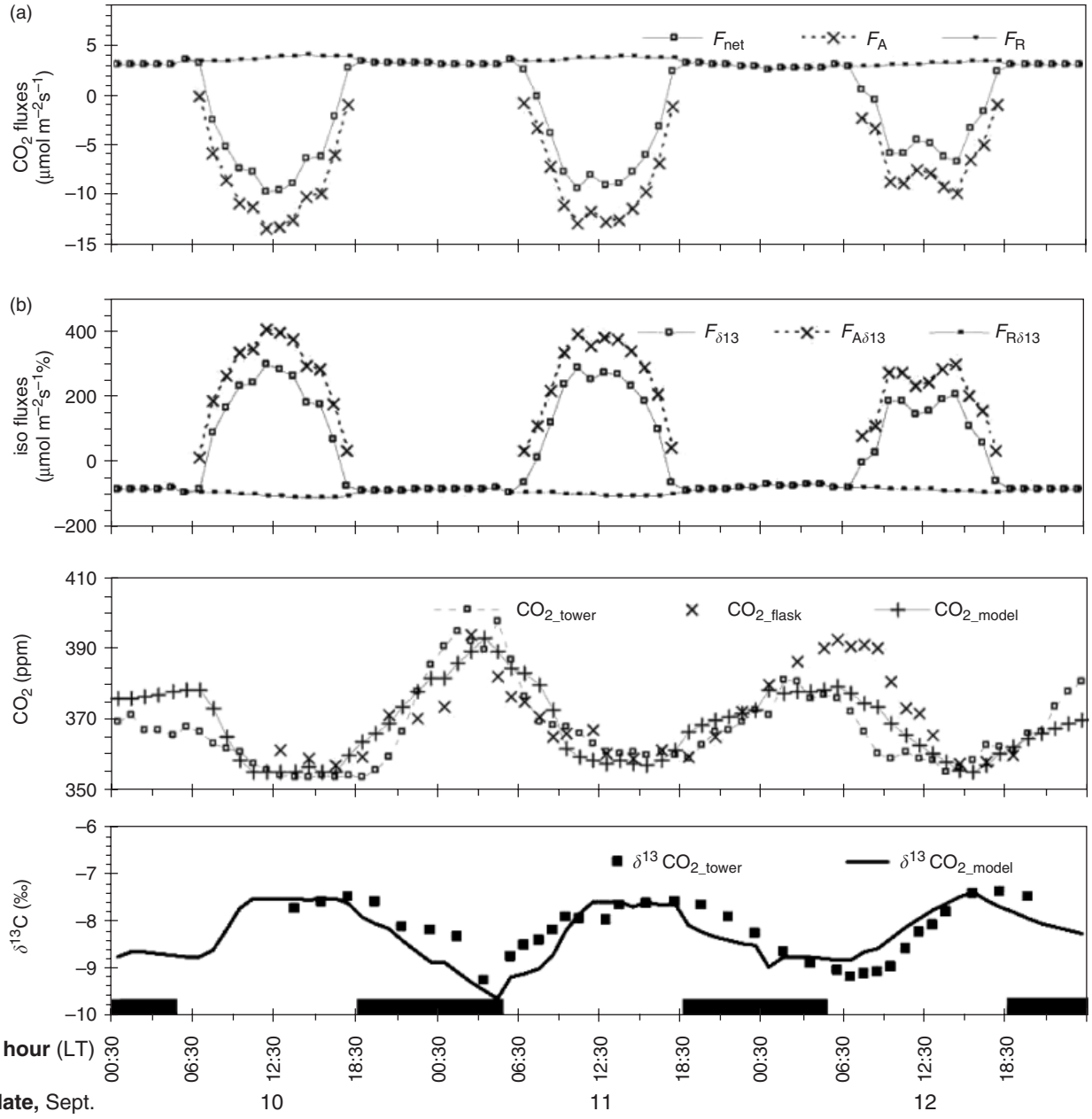

Fig. 8 Same as Fig. 4, but for September 10–12, 1999.

respiration, and the stomata close. Minimum Δ_{canopy} values typically occur during mid-afternoon (14:00–15:00 hours), when the day's highest VPD occur. Moreover, the greatest amplitudes and the lowest mid-afternoon values were modeled to occur in early spring and late summer in a temperate forest ecosystem.

During the growing season in 1999, the mean Δ_{canopy} against $^{13}CO_2$ of a boreal forest ecosystem in the vicinity of the Fraserdale tower was computed to be 19.58‰, but the monthly averages of Δ_{canopy} varied betwen 18.55‰ and 20.84‰ with a seasonal peak during the middle growing season. Both the magnitude and seasonal variation amplitude of Δ_{canopy} for a boreal forest simulated in this study are reasonably smaller than those modeled by Baldocchi & Bowling (2003) for a temperate broad-leaved deciduous forest (19.58‰ vs. 22.4‰; 2.29‰ vs. 9‰). And the simulated seasonal average of Δ_{canopy} in this study is very close to that modeled by Suits *et al*. (2005) for needleleaf forests (19.58‰ vs. 19.2 ± 0.41‰).

The modeled overall seasonal trend of Δ_{canopy} in a boreal forest in the vicinity of the Fraserdale is also

consistent with the measurements made in Douglas-fir forest located on Vancouver Island, British Columbia (49.90°N, 125.37°W): the observed Δ_{canopy} and the carbon isotopic signature of ecosystem respired CO_2 had an increasing trend from the early to middle growing season and a strong decrease at the end of the growing season in 2003 (Ponton *et al*., 2006).

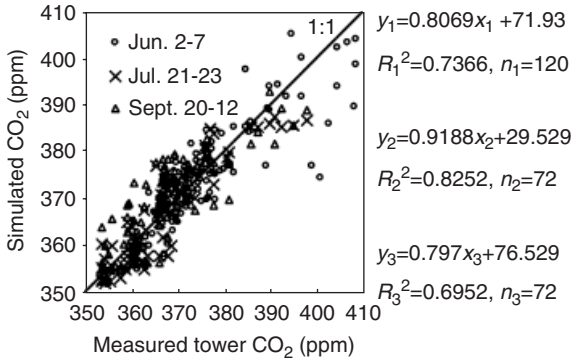

Fig. 9 Linear regression relationships between simulated and measured hourly CO_2 mixing ratio at 20 m height during the growing season in 1999 at Fraserdale, Ontario, Canada. Here y and x represent simulated and observed CO_2 mixing ratio, respectively; R and n denote the linear correlation coefficient and sample number, respectively; subscripts 1–3 denote the campaigns during June 2–7, July 21–23, and September 10–12, respectively.

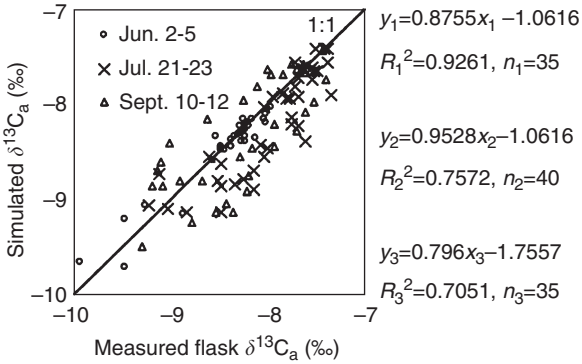

Fig. 10 Same as Fig. 9, but for $\delta^{13}CO_2$.

Seasonal averages of Δ_{canopy} were also estimated using a measurement-based approach by Lai *et al*. (2005a, b) for three biomes: a western coniferous forest (Wind River Canopy Crane Research Facility (WRCCRF), WA, 45.490°N, 121.580°W), an eastern coniferous forest (Howland Forest, ME, 45.150°N, 68.450°W), and a temperate deciduous forest (Harvard Forest, MA, 42.320°N, 72.110°W). The measurement-based estimates of seasonal averaged Δ_{canopy} of 2002 for these three forest biomes are 18.8%, 19.3%, and 20.1%, respectively. The simulated mean Δ_{canopy} of boreal forest ecosystem in the vicinity of the Fraserdale tower (= 19.58‰) is close to measured Δ_{canopy} of coniferous forest ecosystem at WRCCRF and at Howland Forest and is lower than that of temperate deciduous forest at Harvard Forest.

As shown in Fig. 14, there was a significant day-to-day variability in Δ_{canopy} on the basis of the seasonal background values. Δ_{canopy} varied within a range of 3–5‰ at a synoptic scale. The daily mean differences between Δ_{sunlit} and Δ_{shade} were also noticeable with a range of around 0.5 to several permil (Fig. 14). Across hourly to seasonal time scales, Δ_{canopy} and the intrinsic water-use efficiency (the ratio of carbon uptake to water loss) were positively correlated, while Δ_{canopy} negatively responded to vapor pressure deficit and air temperature, and positively responded to air humidity. The interannual variations of Δ_{canopy} in response to meteorological and physiological driving factors in a boreal ecosystem against a 14-year long series data (1990–1996 and 1998–2004) at the study site has also been explored and will be reported elsewhere (Chen & Chen, 2006).

Table 2 Linear regression statistics between modeled and tower observed hourly averaged CO_2 and campaign measured $\delta^{13}CO_2$ in the surface layer (at 20 m height) for three campaign periods in 1999, Fraserdale, Ontario, Canada*

		MBE (ppm, ‰)	RMSE (ppm, ‰)	RMSD (%)	r^2	N
Campaign 1	CO_2	−0.359	4.308	1.155	0.7366	120
(June 2–7)	$\delta^{13}C$	0.007	0.127	1.504	0.9261	35
Campaign 2	CO_2	0.307	4.599	1.252	0.8252	72
(July 21–23)	$\delta^{13}C$	0.112	0.343	4.298	0.7572	40
Campaign 3	CO_2	−1.555	5.024	1.694	0.6952	72
(September 10–-12)	$\delta^{13}C$	0.078	0.393	4.773	0.7051	35

*MBE is the mean bias error, $= \sum_{i=1}^{N} \frac{C_{obs}(i)-C_{mod}(i)}{N}$; RMSE is the root mean square error, $= \sqrt{1/N \sum_{i=1}^{N} [C_{obs}(i) - C_{mod}(i)]^2}$; RMSD is the root mean square difference expressed in percentage of the average of observed CO_2 mixing ratio, $= \frac{RMSE}{|\sum_{i=1}^{N} C_{obs}(i)/ZN|}$; r^2 is the squared linear regression coefficient, $= \frac{N\sum_{i=1}^{N}(C_{obs}(i)C_{mod}(i)) - \sum_{i=1}^{N} C_{obs}(i) \sum_{i=1}^{N} C_{mod}(i)}{\left(N\sum_{i=1}^{N}[C_{obs}(i)]^2 - \left[\sum_{i=1}^{N} C_{obs}(i)\right]^2\right)\left(N\sum_{i=1}^{N}[C_{mod}(i)]^2 - \left[\sum_{i=1}^{N} C_{mod}(i)\right]^2\right)}$.

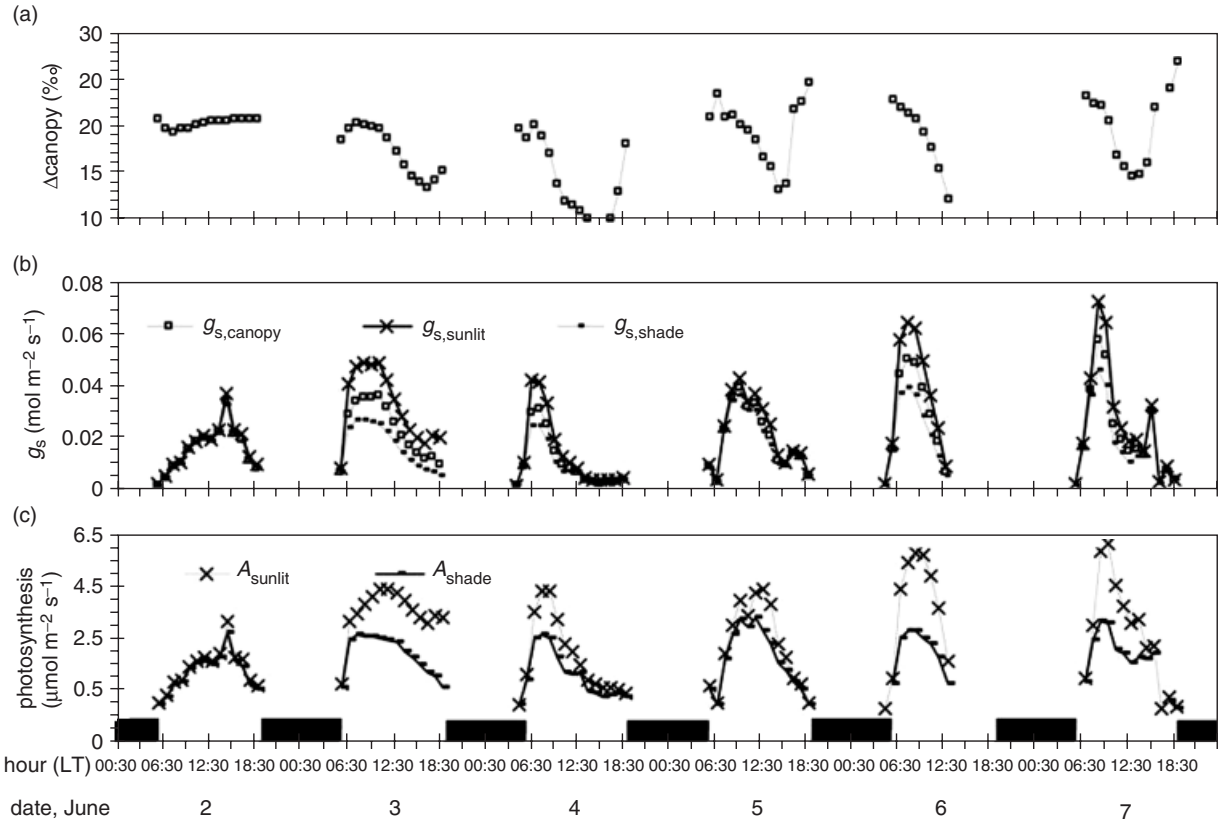

Fig. 11 Modeled canopy isotope discrimination and associated variables during June 2–7, 1999 at Fraserdale tower site. (a) Canopy scale carbon isotope discrimination (Δ_{canopy}); (b) the conductance of CO_2 diffusion from the ambient air to the sites of carboxylation within the chloroplast for the integrated canopy ($g_{s,canopy}$), the sunlit ($g_{s,sunlit}$) and shaded leaves ($g_{s,shade}$); and (c) the photosynthetic CO_2 assimilation rate for sunlit ($A_{s,sunlit}$) and shaded ($A_{s,shade}$) leaves.

Modeled CO_2 fluxes, carbon isotopic fluxes, and $\delta^{13}C$ of CO_2 in the surface layer

The annual total NEE of CO_2, F_A, and F_R were computed, respectively, to be −2.42, −49.48, and 47.06 mol m^{-2} yr^{-1} for the year 1999 at the Fraserdale site. This result is, in agreement with previous work based on remote sensing (Chen *et al*., 2003) and the result derived from tower CO_2 concentration measurements (Chen *et al*., 2006c), boreal ecosystems in the vicinity of this tower were likely a small carbon sink. Correspondingly, $F_{\delta 13}$, $F_{A\delta 13}$, and $F_{R\delta 13}$ were modeled to be 68.30, 1347.25, and −1278.95 mol m^{-2} yr^{-1} ‰, respectively, and note that the true direction of the $^{13}CO_2$ flux due to photosynthesis is downward while that due to respiration is upward. The isoflux associated with the net uptake of CO_2 is positive. If we applied these total annual fluxes to Eqn (7), the annual averages of $\overline{\delta^{13}C_{bio}}$, $\overline{\delta^{13}C_A}$, $\overline{\delta^{13}C_R}$ are approximated to be −28.19‰, −27.22‰, and −27.17‰, respectively, and their respective isotope molar ratios ($^{13}C/^{12}C$) can be estimated using Eqn (4). The annual amounts of ^{13}C associated with NEE of CO_2, F_A and F_R are estimated as the products of fluxes and their respective molar ratios. For the year 1999, the boreal ecosystems in the vicinity of Fraserdale tower sequestrated 77.03 g ^{13}C m^{-2} yr^{-1} due to photosynthesis, released 76.69 g ^{13}C m^{-2} yr^{-1} due to respiration, and consequently net uptake is 0.34 g ^{13}C m^{-2} yr^{-1}. There is obvious seasonality of CO_2 fluxes and isofluxes, as well as of $\delta^{13}C$ of CO_2 at 20 m ($\delta^{13}C_a$) for the year 1999 at Fraserdale site (Fig. 15). During the growing season (May–October), monthly mean F_A varied between −0.1 and −0.38 mol m^{-2} day^{-1} and the maxima occurred during the middle growing season. The seasonal variation of F_R was significant with the maximum of 0.33 mol m^{-2} day^{-1} in July. The NEE of CO_2 (the difference between F_A and F_R) was still negative during the growing season months (i.e. net uptake of carbon). Patterns in isofluxes were similar, with a mid-growing-season peaks of 10.5, −8.5, and 2.6 mol m^{-2} day^{-1} ‰, respectively, for $F_{A\delta 13}$, $F_{R\delta 13}$, and $F_{\delta 13}$. The isofluxes are not simply a linear function of CO_2 fluxes as might be expected from Eqn (7). The strong opposing influences of respiratory and photo-

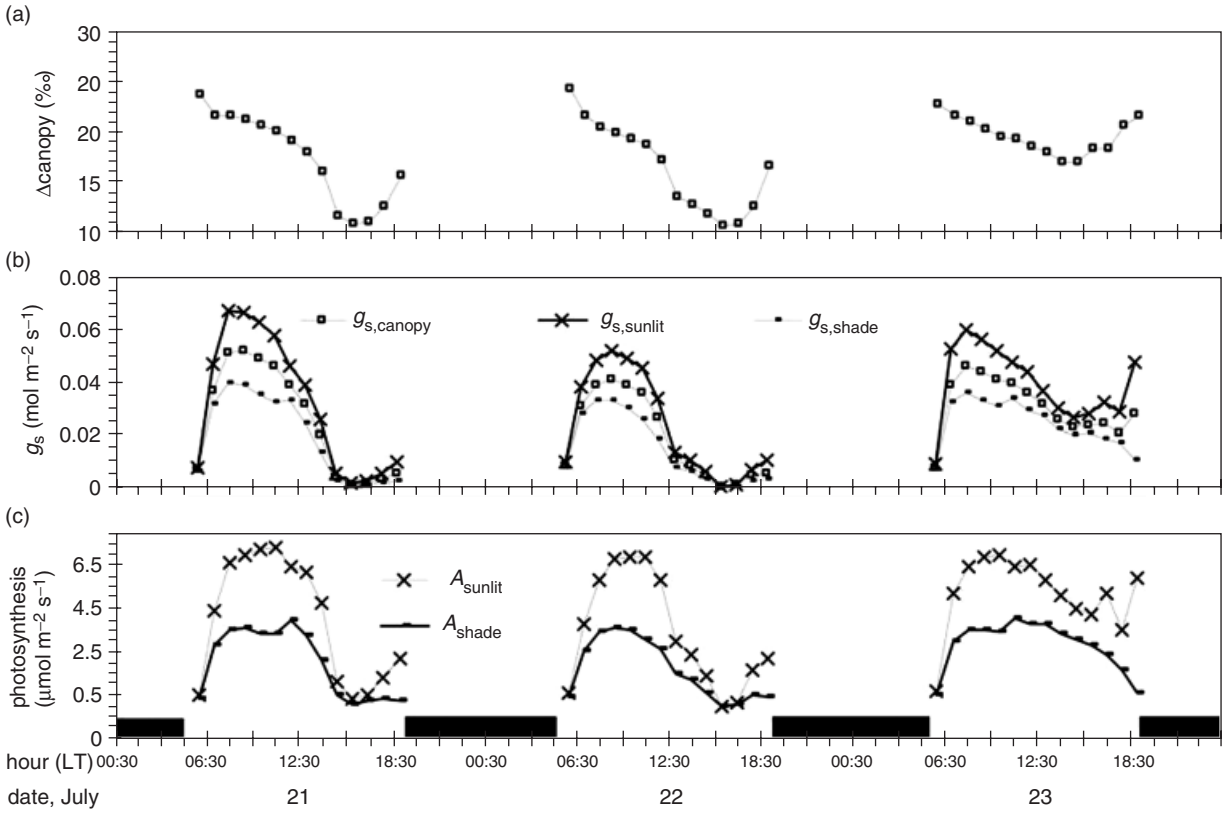

Fig. 12 Same as Fig. 11, but for July 21–23, 1999.

synthetic fluxes on forest air (both CO_2 and $^{13}CO_2$) were apparent. CO_2 was relatively enriched with the heavier ^{13}C isotope (less negative $\delta^{13}C$) from July through October and depleted in the remaining months. At a synoptic scale, there was a significant day-to-day variability in NEE and F_A during the growing season and a small day-to-day variability in F_R (Fig. 15a). Similar signatures were simulated in isofluxes (Fig. 15b). Consistent with the net CO_2 flux and net isoflux ($F_{\delta 13}$), the day-to-day variability in $\delta^{13}C_a$ was more apparent during the growing season than in the nongrowing season (Fig. 15c).

Summary and conclusion

The ecosystem model (BEPS2.0) and the 1-D atmosphere model (VDS) were expanded and coupled to simulate the dynamics of stable carbon isotope of CO_2 exchange between boreal ecosystems and the atmosphere as well as their diffusion processes through the whole CBL. The computed isotopic compositions (i.e. $\delta^{13}C$ values) at the surface layer during the growing season in 1999 at Fraserdale agreed well with intensive campaign data, with the values of r^2 at hourly time steps equal to 0.93, 0.76, and 0.71, for the three campaign periods (which occurred in early, middle and late growing season, respectively). Correspondingly, RMSE values are 0.13‰, 0.34‰, and 0.39‰, respectively, and RMSD values are 1.5%, 4.3%, and 4.8%, respectively.

Modeled diurnal/seasonal patterns and magnitudes of $F_{\delta 13}$, $F_{A\delta 13}$, and $F_{R\delta 13}$ were comparable with existing literature values (e.g. Bowling *et al*., 2001). The annual total $F_{\delta 13}$, $F_{A\delta 13}$, and $F_{R\delta 13}$ were modeled to be 68.30, 1347.25, and −1278.95 mol m^{-2} yr^{-1} ‰, respectively. The annual mean Δ_{canopy} against $^{13}CO_2$ by boreal ecosystems in the vicinity of the Fraserdale tower in 1999 was computed to be 19.58‰, which consistent with both measured and simulated results for similar ecosystems (e.g. Lai *et al*., 2005a, b; Suits *et al*., 2005; Ponton *et al*., 2006). The model diurnal patterns in Δ_{canopy} are also consistent with other estimates in the literature (e.g. Baldocchi & Bowling, 2003).

Factors contributing to the satisfactory performance of the VDS-BEPS2.0 isotope model include its large model domain through the whole CBL, its dependence on coupled and constraining processes, such as leaf energy exchange, turbulent transfer, photosynthesis and stomata conductance, and its representation of these processes on separate sunlit and shaded leaf

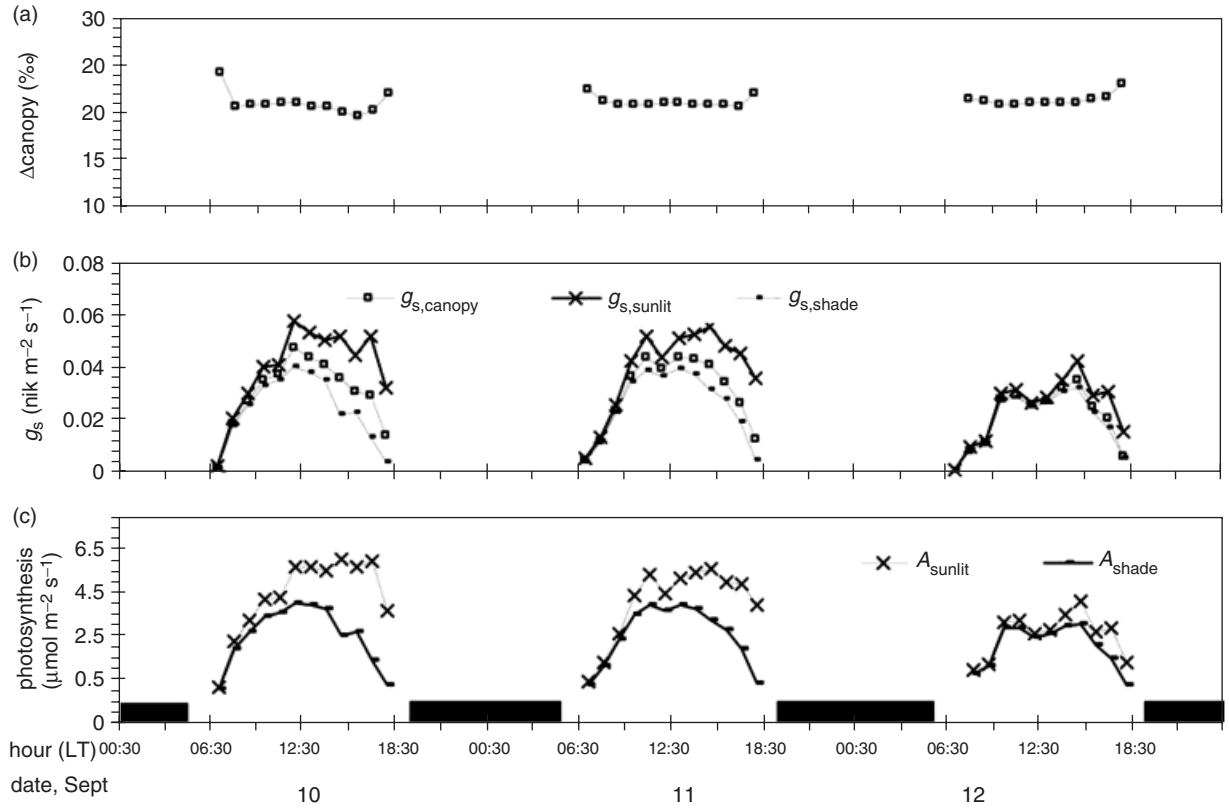

Fig. 13 Same as Fig. 11, but for September 10–12, 1999.

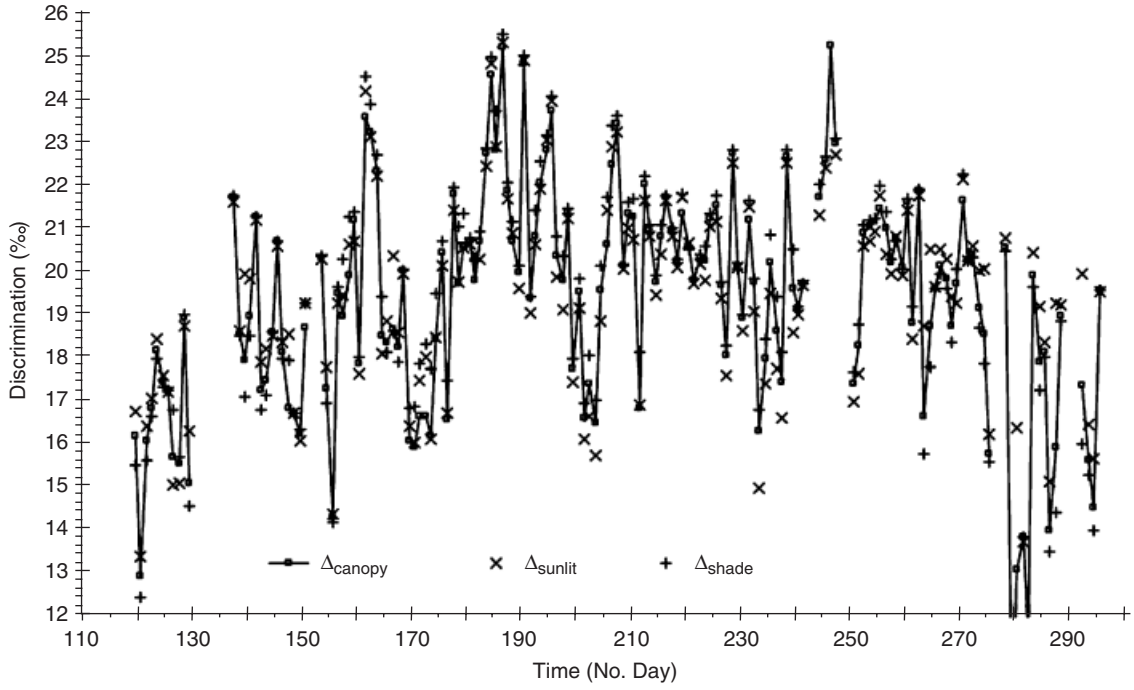

Fig. 14 Simulated daily mean photosynthetic carbon isotope discrimination for the year 1999 at Fraserdale site. The whole-canopy integrated discrimination (Δ_{canopy}) and the discriminations for sunlit leaves (Δ_{sunlit}) and shaded leaves (Δ_{shade}) are shown here for comparison.

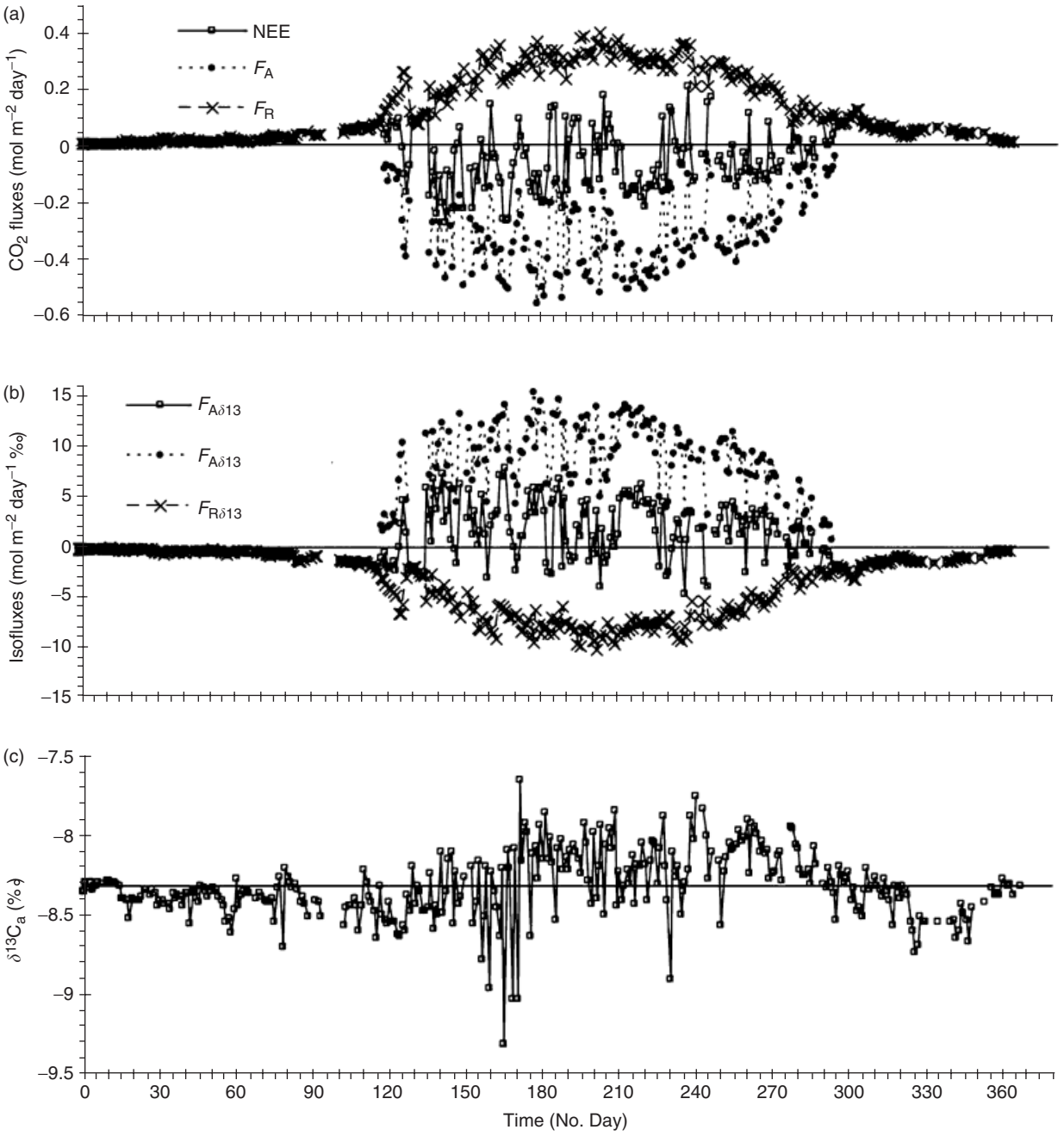

Fig. 15 Simulated seasonal variations in CO_2 fluxes, in isofluxes, and in $\delta^{13}C$ of CO_2 at 20 m ($\delta^{13}C_a$) for the year 1999 at Fraserdale tower site. (a) daily mean CO_2 fluxes, (b) daily mean isofluxes, and (c) daily mean $\delta^{13}C_a$. Note that the true direction of the $^{13}CO_2$ flux is downward during photosynthesis periods. The isoflux associated with the net uptake of $^{13}CO_2$ is positive. The solid horizontal line in panel (c) indicates the annual mean $\delta^{13}C_a$ (= −8.327‰).

classes. This approach contrasts with that of simpler 'big leaf models' (e.g. Lloyd *et al*., 1996), which do not properly consider nonlinear biological combinations of the sunlit and shaded fractions of the canopy. Also this approach differs from most of the existing isotopic biophysical models (e.g. Baldocchi & Bowling, 2003; Ogée *et al*., 2003a) that only focus on the land surface layer without involving the CBL turbulent mixing and entrainment of the air aloft. Moreover, this 'two-leaf' approach is also easy to implement in regional scale GCMs. The VDS-BEPS2.0 isotope model is currently coupled with the global environmental multiscale (GEM) model in order to simulate carbon isotopic exchange between terrestrial ecosystems and the atmo-

sphere at global $1^\circ \times 1^\circ$ resolution through the use of remote sensing and ancillary data.

Regarding future model development and tests, several issues emerge. This physically based model simply treats the isotopic compositions of respired CO_2 owing to autotrophic respiration (by foliage, stem, and roots) and heterotrophic respiration (by soil organisms). Incorporating algorithms that partition soil respiration (or call underground respiration) into root and microbial respiration and available $\delta^{13}C$ values from these C pools will lead to improvements in simulating the isotopic signal from the soil. Some unresolved model issues might have to be deferred until our understanding of the time lags between the period of carbon assimilation and ecosystem respiration is improved (Bowling *et al*., 2002) taking into account isotope disequilibrium. This lag might extend to several days and may vary with tissue (i.e. leaves vs. belowground tissues) (McDowell *et al*., 2004).

Acknowledgement

Authors would like to acknowledge Canadian Foundation for Climate and Atmospheric Sciences (project GC423) and the Climate Change program at Atmospheric Science and Technology Directorate (ASTD), Environment Canada, for financial support of the modeling and measurement work at Fraserdale. The technical contributions by D. Ernst and A. Chivulescu at ASTD for the flask sampling and isotope measurements are appreciated. We would like to acknowledge Doug Worthy and M. Ernst (ASTD) for the measurements of the CO_2 concentration and meteorology data at Faserdale; B. Vaughan, and J. White at INSTAAR, University of Colorado for isotope measurements of the flasks from MBL stations and K. Masarie at the NOAA/CMDL Carbon Cycle Group, for creating and updating the MBL reference fields. This work benefited from useful discussions with Kaz Higuchi, Douglas Chan, and Douglas Worthy of ASTD.

References

Allison CE, Francey RJ, Meijer HAJ (1995) *Recommendations for the reporting of stable isotope measurements of carbon and oxygen in CO_2 gas, in reference and intercomparison materials for stable isotopes of light elements*. IAEA-Tecdoc-825, pp. 155–162.

Bakwin PS, Tans PP, White JWC *et al*. (1998) Determination of the isotopic ($^{13}C/^{12}C$) discrimination by terrestrial biology from a global network of observations. *Global Biogeochemical Cycles*, **3**, 555–562.

Baldocchi DD (1997) Measuring and modelling carbon dioxide and water vapour exchange over a temperate broad-leaved forest during the 1995 summer drought. *Plant, Cell and Environment*, **20**, 1108–1122.

Baldocchi DD, Bowling DR (2003) Modeling the discrimination of ^{13}C above and within a temperate broad-leaved forest canopy on hourly to seasonal time scales. *Plant, Cell and Environment*, **26**, 231–244.

Baldocchi DD, Harley PC (1995) Scaling carbon dioxide and water vapour exchange from leaf to canopy in a deciduous forest: model testing and application. *Plant, Cell and Environment*, **18**, 1157–1173.

Ball JT, Woodrow IE, Berry JA (1987) A model predicting stomatal conductance and its contribution to the control of photosynthesis under different environmental conditions. In: *Progress in Photosynthesis Research* (ed. Biggens J), pp. 221–224. Martinus Nijhoff, Zoetermeer, Netherlands.

Battle MM, Bender L, Tans PP *et al*. (2000) Global carbon sinks and their variability inferred from atmospheric O_2 and $\delta^{13}C$. *Science*, **287**, 2467–2470.

Berry SC, Varney GT, Flanagan LB *et al*. (1997) Leaf $\delta^{13}C$ in Pinus resinosa trees and understory plants: variation associated with light and CO_2 gradients. *Oecologia*, **109**, 499–506.

Bowling DR, Baldocchi DD, Monson RK *et al*. (1999) Dynamics of isotope exchange of carbon dioxide in a Tennessee deciduous forest. *Global Biogeochemical Cycles*, **13**, 903–921.

Bowling DR, McDowell NG, Bond BJ *et al*. (2002) ^{13}C content of ecosystem respiration is linked to precipitation and vapor pressure deficit. *Oecologia*, **131**, 113–124.

Bowling DR, Pataki DE, Ehleringer JR *et al*. (2003a) Critical evaluation of micrometeorological methods for measuring ecosystem–atmosphere isotopic exchange of CO_2. *Agricultural and Forest Meteorology*, **116**, 159–179.

Bowling DR, Sargent SD, Tanner BD *et al*. (2003b) Tunable diode laser absorption spectroscopy for stable isotope studies of ecosystem–atmosphere CO_2 exchange. *Agricultural and Forest Meteorology*, **118**, 1–19.

Bowling DR, Tans PP, Monson RK *et al*. (2001) Partitioning net ecosystem carbon exchange with isotopic fluxes of CO_2. *Global Change Biology*, **7**, 127–145.

Buchmann N, Guehl JM, Barigah TS *et al*. (1997a) Interseasonal comparison of CO_2 concentrations, isotopic composition, and carbon dynamics in an Amazonian rainforest (French Guiana). *Oecolgia*, **110**, 120–131.

Buchmann N, Kao WY, Ehleringer JR *et al*. (1997b) Influence of stand structure on carbon-13 of vegetation, soils, and canopy air within deciduous and evergreen forests in Utah, United States. *Oecologia*, **110**, 109–119.

Chen B, Chen JM (2006) Interannual variation in carbon isotope discrimination in response to meteorological and physiological driving factors in a boreal forest ecosystem. *Global Change Biology*, submitted.

Chen B, Chen JM, Gang M *et al*. (2006a) Modeling and scaling coupled energy, water, and carbon fluxes based on remote sensing: an application to Canada's landmass. *Journal of Hydrometeorology*, accepted.

Chen JM, Chen B, Higuchi K *et al*. (2006c) Boreal ecosystems sequestered more carbon in warmer years. *Geophysical Research Letter*, **33**, L10803, doi:10.1029/2006GL025919.

Chen B, Chen JM, Ju W *et al*. (2006b) Remote sensing based ecosystem-atmosphere simulation scheme (EASS) – model formulation and test with multiple-year data. *Journal of Geophysical Research – Biogeosciences*, revised, submitted.

Chen B, Chen JM, Liu J *et al*. (2004a) A Vertical Diffusion Scheme to estimate the atmospheric rectifier effect. *Journal of Geophysical Research – Atmosphere*, **109**, D04306, doi:10.1029/2003JD003925.

Chen JM, Chen B, Tans PP *et al*. (2004b) Deriving photosynthestic and respiratory fluxes from CO_2 mixing ratio measured on the North Carolina tall tower, AGU 2004 Spring Meeting. *Eos Transactions of AGU*, **85**. *Jt. Assem. Suppl.*, Abstract, 99.

Chen JM, Chen B, Tans PP *et al*. (2006d) Deriving daily carbon fluxes from hourly CO_2 mixing ratios measured on the WLEF tall tower: an upscaling methodology. *Journal of Geophysical Research – Biogeosciences*, submitted.

Chen B, Chen JM, Worthy D *et al*. (2005) Interannual variability in the atmospheric CO_2 rectification over a boreal forest region. *Journal of Geophysical Research – Atmosphere*, **110**, D16301, doi:10.1029/2004JD005546.

Chen DX, Coughenour MB (1994) GEMTM: a general model for energy and mass transfer of land surfaces and its application at the FIFE sites. *Agricultural and Forest Meteorology*, **68**, 145–171.

Chen JM, Ju W, Cihlar J *et al*. (2003) Spatial distribution of carbon sources and sinks in Canada's forests. *Tellus*, **55B**, 622–641.

Chen JM, Liu J, Cihlar J *et al*. (1999) Daily canopy photosynthesis model through temporal and spatial scaling for remote sensing applications. *Ecological Modelling*, **124**, 99–119.

Chen JM, Pavlic G, Brown L *et al*. (2002) Derivation and validation of Canada-wide coarse-resolution leaf area index maps using highresolution satellite imagery and ground measurements. *Remote Sensing of Environment*, **80**, 165–184.

Ciais P, Friedlingstein P, Schimel DS *et al*. (1999) A global calculation of the $\delta^{13}C$ of soil respired carbon: implications for the biospheric uptake of anthropogenic CO_2. *Global Biogeochemical Cycles*, **13**, 519–530.

Ciais P, Tans PP, Trolier M *et al*. (1995a) A large Northern Hemisphere terrestrial CO_2 sink indicated by the $^{13}C/^{12}C$ ratio of atmospheric CO_2. *Science*, **269**, 1098–1102.

Ciais P, Tans PP, White JWC *et al*. (1995b) Partitioning of ocean and land uptake of CO_2 as inferred by $\delta^{13}C$ measurements from NOAA Climate Monitoring and Diagnostics Laboratory Global Air Sampling Network. *Journal of Geophysical Research – Atmosphere*, **100**, 5051–5070.

Cihlar J, Beaubien J, Latifovic R *et al*. (1999) *Land Cover of Canada 1995 Version 1.1. Digital Data Set Documentation*. Natural Resources Canada, Ottawa, Ontario. ftp://ftp2.ccrs.nrcan.gc.ca/ftp/ad/EMS/landcover95/.

Condon AG, Richards RA, Farquhar GD *et al*. (1993) Relationship between carbon isotope discrimination, water use efficiency and transpiration efficiency for dryland wheat. *Australia Journal Agriculture Research*, **44**, 1693–1711.

Conway TJ, Tans PP, Waterman LS *et al*. (1994) Evidence for interannual variability of the carbon cycle from the NOAA/CMDL global air sampling network. *Journal of Geophysical Research – Atmosphere*, **99**, 22831–22855, (data updates available from www.cmdl.noaa.gov/ccgg/).

Cowan IR (1977) Stomatal behaviour and environment. *Advances in Botanical Research*, **4**, 117–228.

Cowan IR (1982) Regulations and water use in relation to carbon gain in higher plants. In: *Encyclopedia of Plant Ecophysiology, New Series*, Vol. 12B (eds Lange L, Nobel PS, Osmond CB), pp. 589–613. Springer-Verlag, New York.

Craig H (1953) Carbon-13 in plants and the relationships between carbon-13 and carbon-14 variations in nature. *Journal of Geology*, **62**, 115–149.

Ekblad A, Högberg P (2001) Natural abundance of ^{13}C in CO_2 respired from forest soils reveals speed of link between tree photosynthesis and root respiration. *Oecologia*, **127**, 305–308.

Enting IG, Trudinger CM, Francey RJ *et al*. (1995) A synthesis inversion of the concentration and $\delta^{13}C$ of atmospheric CO_2. *Tellus*, **47B**, 35–52.

Farquhar GD, Ehleringer JR, Hubick KT *et al*. (1989) Carbon isotope discrimination and photosynthesis. *Annual Review of Plant Physiology and Plant Molecular Biology*, **40**, 503–537.

Farquhar GD, Hubick KT, Condon AG *et al*. (1988) Carbon isotope discrimination and plant water use efficiency. In: *StableIsotopes in Ecological Research* (eds Rundel PW *et al*.), pp. 21–40. Academic Press, San Diego, CA.

Farquhar GD, Lloyd J (1993) Carbon and oxygen isotope effects in the exchange of carbon dioxide between terrestrial plants and the atmosphere. In: *Stable Isotopes and Plant Carbon–Water Relations* (eds Ehleringer JR, Hall AE, Farquhar GD), pp. 47–70. Academic Press, San Diego, CA.

Farquhar GD, O'Leary MH, Berry JA *et al*. (1982) On the relationship between carbon isotope discrimination and the intercellular carbon dioxide concentration in leaves. *Australian Journal of Plant Physiology*, **9**, 121–137.

Farquhar GD, Richards RA (1984) Isotopic composition of plant carbon correlates with water-use efficiency of wheat genotypes. *Australia Journal Plant Physiology*, **11**, 539–552.

Farquhar GD, von Caemmerer S, Berry JA *et al*. (1980) A biochemical model of photosynthetic CO_2 assimilation in leaves of C3 species. *Planta*, **149**, 78–90.

Flanagan LB, Brooks JR, Varney GT *et al*. (1996) Carbon isotope discrimination during photosynthesis and the isotope ratio of respired CO_2 in boreal forest ecosystems. *Global Biogeochemical Cycles*, **10**, 629–640.

Francey RJ, Tans PP, Allison CE *et al*. (1995) Changes in oceanic and terrestrial carbon uptake since 1982. *Nature*, **373**, 326–330.

Fung IY, Berry JA, Field CB *et al*. (1997) Carbon 13 exchanges between the atmosphere and the biosphere. *Global Biogeochemical Cycles*, **11**, 507–533.

GLOBALVIEW-CO_2 (2005) Cooperative Atmospheric Data Integration Project: Carbon Dioxide (CD-ROM), NOAA Clim. Monit. and Diag. Lab., Boulder, CO (available via anonymous FTP to ftp.cmdl.noaa.gov, Path: ccg/co2/GLOBALVIEW).

Griffis TJ, Baker JM, Sargent SD *et al*. (2004) Measuring field-scale isotopic CO_2 fluxes with tunable diode laser absorption spectroscopy and micrometeorological techniques. *Agricultural and Forest Meteorology*, **124**, 15–29.

Griffis TJ, Baker JM, Zhang J *et al*. (2005) Seasonal dynamics and partitioning of isotopic CO_2 exchange in a C_3/C_4 managed ecosystem. *Agricultural and Forest Meteorology*, **132**, 1–19.

Hall AE, Ismail AM, Menendez CM (1993) Implications for plant breeding of genotypic and drought induced differences in water use efficiency, carbon isotope discrimination and gas exchange. In: *Stable Isotopes and Plant Carbon–Water Relations* (eds Ehleringer JR, Hall AE, Farquhar GD), pp. 19–28. Academic Press, San Diego, CA.

Hersterberg R, Siegethaler U (1991) Production and stable isotopic composition of CO_2 in a soil near Bern, Switzerland. *Tellus*, **43B**, 197–205.

Higuchi K, Worthy D, Chan D *et al*. (2003) Regional source/sink impact on the diurnal, seasonal and inter-annual variations in atmospheric CO_2 at a boreal forest site in Canada. *Tellus*, **55B**, 115–125.

Huang L, Norman AL, Allison CE, Francey RJ, Ernst D, Chivulescu A, Higuchi K (2003) Traceability–maintenance for high precision stable isotope measurement ($\delta^{13}C$ & $\delta^{18}O$) of Air-CO_2 by Lab-Carbonate-Standards at MSC: application to the Inter-Comparision Program (alert, Canada) with CSIRO. In: *The Report to the 11th WMO/IAEA Meeting of Experts on CO_2 Concentration and Related Tracer Measurement Techniques*. Tokyo, Japan September 2001, No. 148, 9–16.

Jarvis PG (1976) The interpretation of the variations in leaf water potential and stomatal conductance found in canopies in the field. *The Royal Society of London, Philosophical Transactions Series B*, **273**, 593–610.

Keeling CD (1961) A mechanism for cyclic enrichment of carbon-12 by terrestrial plants, Geochim. *Cosmochimica Acta*, **24**, 299–313.

Keeling CD, Piper SC, Bacastor RB *et al*. (2001) *Exchanges of Atmospheric CO_2 and $^{13}CO_2$ with the Terrestrial Biosphere and Oceans from 1978 to 2000: I. Global Aspects, SIO Reference Series 01-06* pp. 1–45. Scripps Institute of Oceanography, San Diego, CA.

Keeling CD, Piper SC, Heimann M (1989) A three-dimensional model of atmospheric CO_2 transport based on observed winds: 4. Mean annual gradients and interannual variations. In: *Aspects of Climate Variability in the Pacific and Western Americas, Geophysics Monographs Series*, Vol. 55 (ed. Peterson DH), pp. 305–363. AGU, Washington, DC.

Knohl A, Buchmann N (2005) Partitioning the net CO_2 flux of a deciduous forest into respiration and assimilation using stable carbon isotopes. *Global Biogeochemical Cycles*, **19**, GB4008, doi:10.1029/2004GB002301.

Lacelle B (1998) Canada's soil organic carbon database. In: *Soil Processes and the Carbon Cycle* (eds Lal R, Kimbla J, Follett RF, Stewart BA), pp. 81–92. CRC Press, Boca Raton, FL.

Lai CT, Ehleringer J, Schauer A *et al*. (2005a) Canopy-scale δ13C of photosynthetic and respiratory CO_2 fluxes: observations in forest biomes across the United States. *Global Change Biology*, **11**, 633–643, doi:10.1111/j.1365-2486.2005.00931.x.

Lai CT, Ehleringer J, Schauer A *et al*. (2005b) Canopy-scale $\delta^{13}C$ of photosynthetic and respiratory CO_2 fluxes: observations in forest biomes across the United States. *Global Change Biology*, **11**, 633–643, doi:10.1111/j.1365-2486.2005.00931.x.

Lai CT, Ehleringer JR, Tans PP *et al*. (2004) Estimating photosynthetic ^{13}C discrimination in terrestrial CO_2 exchange from canopy to regional scales. *Global Biogeochemical Cycles*, **18**, GB1041, doi:10.1029/2003GB002148.

Lai CT, Katul G, Oren R *et al*. (2000) Modeling CO_2 and water vapor turbulent flux distributions within a forest canopy. *Journal of Geophysical Research – Atmosphere*, **105**, 26333–26351.

Lai CT, Riley W, Owensby C *et al*. (2006) Seasonal and interannual variations of carbon and oxygen isotopes of respired CO_2 in a tallgrass prairie: measurements and modeling results from three years with contrasting water availability. *Journal of Geophysical Research – Atmosphere*, **111**, D08506, doi:10.1029/2005JD006436.

Lai CT, Schauer AJ, Owensby C *et al*. (2003) Isotopic air sampling in a tallgrass prairie to partition net ecosystem CO_2 exchange. *Journal of Geophysical Research – Atmosphere*, **108**, 4566, doi:10.1029/2002JD003369.

Le Roux X, Bariac T, Sinoquet H *et al*. (2001) Spatial distribution of leaf water use efficiency and carbon isotope discrimination within an isolated tree crown. *Plant Cell Environment*, **24**, 1021–1032.

Leuning R (1995) Acritical appraisalof a combined stomatal-photosynthesis model for C3 plants. *Plant Cell Environment*, **6**, 181–194.

Leuning R (2000) Estimation of scalar source/sink distributions in plant canopies using Lagrangian dispersion analysis: corrections for atmospheric stability and comparison with a multilayer canopy model. *Boundary Layer Meteorology*, **96**, 293–314.

Liu J, Chen JM, Cihlar J *et al*. (1997) A process-based boreal ecosystem productivity simulator using remote sensing inputs. *Remote Sensing of Environment*, **62**, 158–175.

Liu J, Chen JM, Cihlar J *et al*. (1999) Net primary productivity distribution in BOREAS region from a process model using satellite and surface data. *Journal of Geophysical Research – Atmosphere*, **104**, 27735–27754.

Liu J, Chen JM, Cihlar J *et al*. (2002) Net primary productivity mapped for Canada at 1-km resolution. *Global Ecology and Biogeography*, **11**, 115–129.

Lloyd J, Francey RJ, Mollicone D *et al*. (2001) Vertical profiles, boundary layer budgets, and regional flux estimates for CO_2 and its $^{13}C/^{12}C$ ratio and for water vapor above a forest/bog mosaic in central Siberia. *Global Biogeochemical Cycles*, **15**, 267–284.

Lloyd J, Kruijt B, Hollinger DY *et al*. (1996) Vegetation effects on the isotopic composition of atmospheric CO_2 at local and regional scales: theoretical aspects and a comparison between rain forest in Amazonia and a boreal forest in Siberia. *Australian Journal of Plant Physiology*, **23**, 371–399.

Masarie KA, Tans PP (1995) Extension and integration of atmospheric carbon dioxide data into a globally consistent measurement record. *Journal of Geophysical Research – Atmosphere*, **100**, 593–1610.

Matsushita B, Tamura M (2002) Integrating remotely sensed data with an ecosystem model to estimate net primary productivity in East Asia. *Remote Sensing of Environment*, **81**, 58–66.

McDowell NG, Bowling DR, Bond BJ *et al*. (2004) Response of the carbon isotopic content of ecosystem, leaf, and soil respiration to meteorological and physiological driving factors in a Pinus ponderosa ecosystem. *Global Biogeochemical Cycles*, **18**, GB1013, doi:10.1029/2003GB002049.

McManus JB, Nelson DD, Shorter JH *et al*. (2005) A high precision pulsed quantum cascade laser spectrometer for measurements of stable isotopes of carbon dioxide. *Journal of Modern Optics*, **52**, 2309–2321.

Miller JB, Tans PP (2003) Calculating isotopic fractionation from atmospheric measurements at various scales. *Tellus*, **55B**, 207–214.

Miller JB, Tans PP, White JWC *et al*. (2003) The atmospheric signal of terrestrial carbon isotopic discrimination and its implication for partitioning carbon fluxes. *Tellus*, **55B**, 197–206.

Monteith JL (1995) A reinterpretation of stomatal responses to humidity. *Plant Cell Environment*, **18**, 365–372.

Moreira M, Sternberg L, Martinelli L *et al*. (1997) Contribution of transpiration to forest ambient vapour based on isotopic measurements. *Global Change Biology*, **3**, 439–450.

Norman JM (1980) Interfacing leaf and canopy light interception models. In: *Predicting Photosynthesis for Ecosystem Models* (eds Hesketh JD, Jones JW), pp. 49–68. CRC, Boca Raton, FL.

Norman JM (1982) Simulation of microclimates. In: *Biometeorology in Integrated Pest Management* (eds Hatfield JL, Thomason IJ), pp. 65–99. Academic Press, New York.

Ogée J, Brunet Y, Loustau D *et al*. (2003a) MuSICA, a CO_2, water and energy multi-layer, multi-leaf pine forest model: evaluation from hourly to yearly time scales and sensitivity analysis. *Global Change Biology*, **9**, 697–717.

Ogée J, Peylin P, Ciais P *et al*. (2003b) Partitioning net ecosystem carbon exchange into net assimilation and respiration using $^{13}CO_2$ measurements: a cost-effective sampling strategy. *Global Biogeochemical Cycles*, **17**, 1070, doi:10.1029/2002GB001995.

Parton WJ, Ojima DS, Cole CV *et al*. (1993) A general model for soil organic matter dynamics: sensitivity to litter chemistry, texture and management (special publication). *Soil Science Society of America Journal*, **39**, 147–167.

Pataki DE, Ehleringer JR, Flanagan LB *et al*. (2003) The application and interpretation of Keeling plots in terrestrial carbon cycle research. *Global Biogeochemical Cycles*, **17**, 1022 doi:10.1029/2001GB001850.

Ponton S, Flanagan LB, Alstard K *et al*. (2006) Comparison of ecosystem water-use efficiency among Douglas-fir forest, aspen forest and grassland using eddy covariance and carbon isotope techniques. *Global Change Biology*, **12**, 294–310.

Potosnak MJ, Wofsy SC, Denning AS (1999) Influence of biotic exchange and combustion sources on atmospheric CO_2 concentration in New England from observations at a forest flux tower. *Journal of Geophysical Research-Atmosphere*, **104**, 9561–9569.

Raupach MR, Finnigan JJ (1988) Single-layer models of evaporation from plant canopies are incorrect but useful, whereas, multilayer models are correct but useless. *Discussion Australia Journal Plant Physiology*, **15**, 705–716.

Rayner PJ, Enting IG, Francey RJ *et al*. (1999) Reconstructing the recent carbon cycle from atmospheric CO_2, $\delta^{13}C$ and O_2/N_2 observations. *Tellus*, **51B**, 213–232.

Running SW, Coughlan JC (1988) A general model of forest ecosystem processes for regional applications I. Hydrological balance, canopy gas exchange and primary production processes. *Ecological Model*, **42**, 125–154.

Ryan MG (1991) A simple method for estimating gross carbon budgets for vegetation in forest ecosystems. *Tree Physiology*, **9**, 255–266.

Schauer AJ, Lott MJ, Cook CS *et al*. (2005) An automated system for stable isotope and concentration analyses of CO_2 from small atmospheric samples. *Rapid Communications in Mass Spectrometry*, **19**, 359–362.

Schleser GH, Jayasekera R (1985) $\delta^{13}C$ variations of leaves in forests as an indication of reassimilated CO_2 from the soil. *Oecologia*, **65**, 536–542.

Schulze ED, Ellis R, Schulze W *et al*. (1996) Diversity, metabolic types and $\delta^{13}C$ carbon isotope ratios in grass flora of Namibia in relation to growth form, precipitation and habitat conditions. *Oecologia*, **106**, 352–369.

Schulze ED, Williams RJ, Farquhar GD *et al*. (1998) Carbon and nitrogen isotope discrimination and nitrogen nutrition of trees along a rainfall gradient in northern Australia. *Australia. Journal Plant Physiolology*, **25**, 413–425.

Schut P, Shields J, Tarnocai C *et al*. (1994) Soil landscapes of Canada – an environmental reporting tool. *Canadian Conference on GIS Proceedings*, June 6–10, 1994, Ottawa, pp. 953–965.

Sellers PJ, Dickinson RE, Randall DA *et al*. (1997) Modeling the exchange of energy, water, and carbon between continentals and the atmosphere. *Science*, **275**, 502–509.

Shields JA, Tarnocai C, Valentine KWG, MacDonald KB (1991) Soil landscapes of Canada, procedures manual and user's hand book, *Agric. Can. Publ. 1868/E, Agric. Can.*, Ottawa, ON, Canada.

Sternberg LSLO (1989) A model to estimate carbon dioxide recycling in forests using $^{13}C/^{12}C$ ratios and concentrations of ambient carbon dioxide. *Agricultural and Forest Meteorology*, **48**, 163–173.

Sternberg LSO, Moreira MZ, Martinelli LA *et al*. (1997) Carbon dioxide recycling in two Amazonian tropical forests. *Agricultural and Forest Meteorology*, **88**, 259–268.

Suits NS, Denning AS, Berry JA *et al*. (2005) Simulation of carbon isotope discrimination of the terrestrial biosphere. *Global Biogeochemical Cycles*, **19**, GB1017, doi:10.1029/2003GB002141.

Sun R, Chen JM, Zhou Y *et al*. (2004) Estimation of net primary productivity and evapotranspiration in Changbaishan, China using ETM data. *Canadian Journal of Remote Sensing*, **30**, 731–742.

Tans PP (1980) On calculating the transfer of carbon-13 in reservoir models of the carbon cycle. *Tellus*, **32B**, 464–469.

Tans PP, Berry JA, Keeling RF *et al*. (1993) Oceanic $^{13}C/^{12}C$ observations: a new window on ocean CO_2 uptake. *Global Biogeochemical Cycles*, **7**, 353–368.

Tans PP, Fung IY, Takahashi T *et al*. (1990) Observation constraints on the global atmospheric CO_2 budget. *Science*, **247**, 1431–1438.

Thom M, Bosinger R, Schimdt M *et al*. (1993) The regional budget of atmospheric methane of a highly populated area. *Chemosphere*, **26**, 143–160.

Trolier M, White JWC, Tans PP *et al*. (1996) Monitoring the isotopic composition of atmospheric CO_2: measurements from the NOAA global air sampling network. *Journal of Geophysics Research – Atmosphere*, **101**, 25897–25916.

Wang Q, Tenhunen J, Falge E *et al*. (2003) Simulation and scaling of temporal variation in gross primary production for coniferous and deciduous temperate forests. *Global Change Biology*, **10**, 37–51, doi:10.1046/j.1529-8817.2003.00716.x.

Yakir D, Wang XF (1996) Fluxes of CO_2 and water between terrestrial vegetation and the atmosphere estimated from isotope measurements. *Nature*, **380**, 515–517.

Appendix A: Expansions in BEPS2.0

BEPS is a 1-D, remote sensing based, 'two leaf' (sunlit and shade leaves) biosphere-atmosphere gas exchange model, which is originally developed for Canada's ecosystems in daily time step (Liu *et al*., 1999, 2002). Daily-step BEPS has been updated to hourly step version 2.0 by including a land surface scheme (namely ecosystem–atmosphere simulation scheme) as a crucial component, in that exchanges of energy and water and carbon assimilation are fully coupled (Chen *et al*., 2006a, b).

Much advance has been made in our understanding of biochemical processes at the leaf level, which is fundamental for ecosystem model construction, such as photosynthesis (Farquhar *et al*., 1980, 1982), stomatal behavior, and biophysics of transpiration (Jarvis, 1976; Cowan, 1977, 1982; Ball *et al*., 1987; Monteith, 1995). Many ecosystem models have been integrated from individual leaf-level processes using different up-scaling strategies: (i) 'big-leaf' canopy model (e.g. Raupach & Finnigan, 1988; Leuning, 1995; Sellers *et al*., 1997); (ii) 'multilayer' canopy model (Baldocchi & Harley, 1995; Baldocchi, 1997); (iii) 'two-leaf' canopy model (Norman, 1980; Chen & Coughenour, 1994; Liu *et al*., 1999); and (iv) 'multilayer and multileaf' canopy model (Lai *et al*., 2000; Ogée *et al*., 2003a).

However, there exists a challenge in formulating an isotope ecosystem model, i.e. how to scale up from carbon isotopic discrimination processes at the leaf level (Farquhar *et al*., 1982, 1989; Farquhar & Lloyd, 1993). Few isotope biophysical models have used the 'multilayer' strategy (Lloyd *et al*., 1996; Baldocchi & Bowling, 2003a; Ogée *et al*., 2003a) or 'big-leaf' strategy (Bowling *et al*., 2001; Lai *et al*., 2003). Yet, a 'two-leaf' carbon isotope canopy model has not appeared in the literature, to our knowledge.

A 'two-leaf' carbon isotope canopy model was done in this study within BEPS2.0 (i.e. BEPS-EASS) in order to reduce model complexity from the 'multilayer' formulation and to avoid shortcomings of the 'big-leaf' canopy model shown by Chen *et al*. (1999). Such a two-leaf isotopic bio-physiology model can be easily implemented in GCMs. Expansions made in BEPS2.0 were focused on the solution for Eqn (7), which are briefly overviewed below.

Modeling total canopy photosynthetic assimilation, F_A

The photosynthetic CO_2 assimilations for individual sunlit and shaded leaves, A_{sunlit} and A_{shade}, are modeled on the basis of mechanistic model of Farquhar *et al*. (1980) for C3 plants and coupled with a stomatal conductance model (Liu *et al*., 1999), with separate calculations for sunlit and shaded leaves. The net carbon assimilation for sunlit leaves (F_{sunlit}) and shaded leaves (F_{shade}), can be calculated, respectively, by the sunlit and shaded proportion of total tree LAI (in $m^2\,m^{-2}$) (Norman, 1982):

$$F_{sunlit} = A_{sunlit}\ LAI_{sunlit}, \tag{A1a}$$

$$F_{shade} = A_{shade}\ LAI_{shade}. \tag{A1b}$$

The total canopy net assimilation (F_A) is the sum of these two components,

$$F_A = F_{sunlit} + F_{shade}. \tag{A2}$$

Partition of the total LAI into sunlit and shaded portions is a function of cosine of solar zenith angle (β_z) and clumping index (Ω, unitless with a range from 0 to 1; for conifer in this study, we take the value of 0.5) (Norman, 1982; Chen *et al*., 1999),

$$LAI_{sunlit} = 2\cos\beta_z[1 - \exp(-0.5\Omega LAI/\cos\beta_z)], \tag{A3a}$$

$$LAI_{shade} = LAI - LAI_{sunlit}. \tag{A3b}$$

Modeling whole-canopy photosynthetic discrimination, Δ_{canopy}

The photosynthetic discrimination against $^{13}CO_2$ at the leaf level (Δ, in per mil, ‰) was computed according to previous methods (Farquhar *et al*., 1989; Farquhar & Lloyd, 1993; Lloyd *et al*., 1996) with explicit consideration of unit equality,

$$\Delta = b - \frac{(b-a)A}{g_s C_a}\frac{RT}{p}, \tag{A4}$$

where b is the net fractionation of the enzyme-catalyzed fixation of CO_2 ranging from 26.4‰ to 28.2‰ for C3 plants (Lloyd *et al*., 1996) (b is set to be 27.4‰ in this study), a is the fractionation resulting from the diffusion of CO_2 between the canopy air space and the sites of carboxylation in leaves (= 4.4‰, (Craig, 1953)); g_s represents the conductance to CO_2 diffusion from the ambient air to the sites of carboxylation within the chloroplast, in $m\,s^{-1}$; C_a is the CO_2 mole fraction of ambient air in the canopy in $\mu mol\,mol^{-1}$; A is the photosynthetic CO_2 assimilation rate in $\mu mol\,m^{-2}\,s^{-1}$; R is the universal gas constant in $Pa\,m^3\,K^{-1}\,mol^{-1}$; T is the air temperature in K; and p is the air pressure in Pa.

The BEPS2.0 isotope model with the separation of sunlit and shaded leaves, improves its accuracy in

carbon isotopic flux calculation because of significant difference in photosynthetic discrimination against $^{13}CO_2$ between sunlit and shaded leaves. The g_s for sunlit leaves ($g_{s,\ sunlit}$) and shaded leaves ($g_{s,\ shade}$) has different values, which can be calculated by a combined function of RAD, T_a, VPD, and soil moisture, such as that in Liu *et al*. (1999). Substituting $g_{s,\ sunlit}$, A_{sunlit} and $g_{s,\ shade}$, $A_{shadeit}$ in Eqn (A4), we can gain photosynthetic discrimination for sunlit leaves (Δ_{sunlit}) and shaded leaves (Δ_{shade}). The Δ_{canopy} might be the flux-weighted average of net carbon assimilation for sunlit leaves (F_{sunlit}) and shaded leaves (F_{shade}):

$$\Delta_{canopy} = \frac{\Delta_{sunlit}F_{sunlit} + \Delta_{shade}F_{shade}}{F_A}, \qquad (A5)$$

where F_{sunlit}, F_{shade}, and the total canopy net assimilation (F_A) are calculated using Eqns (A1–A3).

By now, if we know the CO_2 mole fraction of the ambient air (C_a) and its isotopic composition ($\delta^{13}C_a$), the isotopic flux due to photosynthetic carbon discrimination, that is, $(\delta^{13}C_a - \Delta_{canopy})F_A$, can be calculated by combining Eqns A1–A5. C_a and $\delta^{13}C_a$ are approximated as the values simulated at 20 m height simulated by VDS (see Appendix B). The remaining task is then to determine the isotopic flux due to respired CO_2.

Modeling total ecosystem respiration, F_R

Conventionally, autotrophic respiration (R_a) is separated into maintenance respiration (R_m) and growth respiration (R_g) (Running and Coughlan 1988; Ryan 1991),

$$R_a = R_m + R_g = \sum_j (R_{m,j} + R_{g,j}), \qquad (A6)$$

where j is an index for different plant components (1 for leaf, 2 for stem, and 3 for root). Maintenance respiration is temperature dependent, which is determined using Q_{10} equation (Liu *et al*., 1999). Growth respiration is generally considered to be independent of temperature and is proportional to GPP (Liu *et al*., 1999). R_h is calculated as the sum of heterotrophic respiration from different carbon pools and soil layers. The equation contains temperature- and moisture-dependent respiration coefficients for the different pools (Chen *et al*., 2003). For each carbon pool, the respiration coefficient for the jth pool (K_j) was calculated by (Parton *et al*., 1993)

$$K_j = K_{j\_max} f_t(T_s) f_\theta(\theta), \qquad (A8)$$

where K_{j_max} is the maximum respiration rate coefficient for the jth pool; T_s and θ are, respectively, temperature and moisture volumetric content of the soil layers that host the jth pool.

The isotopic composition of respired CO_2 *(*$\delta^{13}C_R$, $\delta^{13}C_R^h$ *and* $\delta^{13}C_R^a$*)*

The isotopic composition of respired CO_2, $\delta^{13}C_R$, is crucial for modeling the isotopic flux caused by respiration. To determine $\delta^{13}C_R$, several methods can be used (Lloyd *et al*., 1996). One is to examine the isotopic composition of respiring materials such as living organic material (i.e. leaves, trunks, roots, moss) and dead organic material (i.e. litter, soil organic matter, different soil carbon pools) (Sternberg, 1989). Nevertheless, one should reasonably consider the isotope fractionation during respiration (Farquhar & Lloyd, 1993). The second option is to measure the respiratory sources directly (e.g. soil CO_2; Hersterberg & Siegethaler, 1991). And the third option is to use the Keeling plot against measured data of CO_2 concentration and $^{13}CO_2$ during nighttime. In the present study, the carbon isotopic compositions of ecosystem respiration, $\delta^{13}C_R$ was calculated from all the nighttime data in the campaigns (1998–2000), using Eqn (5). On the basis of the discrete $\delta^{13}C_R$ in 1999 and the reference values in 2000 and 1998, we gain monthly values of $\delta^{13}C_R$ for 1999 using series-interpolation technique (Fig. 1). At first model test run, monthly $\delta^{13}C_R$, one of the predetermined parameters for calculating the isotopic flux caused by respiration, is approximated as the values $\delta^{13}C_R^h$ and of $\delta^{13}C_R^a$. Once we gain the primary results, the monthly mean value of carbon isotopic composition of new fixed carbon during growing season, $\overline{\delta^{13}C_A}$, can be calculated,

$$\overline{\delta^{13}C_A} = \overline{\delta^{13}C_a} - \overline{\Delta_{canopy}}. \qquad (A9)$$

The monthly mean values of $\overline{\delta^{13}C_R^a}$ during growing season months are assumed to be equal to the specific month values of $\overline{\delta^{13}C_A}$ and for the nongrowing season, the isotopic composition of maintenance respiration $\overline{\delta^{13}C_R^m} = \overline{\delta^{13}C_R^a}$ can be calculated using Eqn (A9) by replacing monthly mean $\overline{\Delta_{canopy}}$ with its annual mean value. Briefly, we gain monthly mean values of $\delta^{13}C_R^h$ and $\overline{\delta^{13}C_R^a}$ for the final model run by assuming that $\delta^{13}C_R^h \approx \overline{\delta^{13}C_R}$ and $\overline{\delta^{13}C_R^a} \approx \overline{\delta^{13}C_A}$ (Fig. 1). Once we gain the solutions for $\delta^{13}C_R^h$, $\overline{\delta^{13}C_R^a}$, R_a, and R_h, the isotopic flux caused by respiration can be calculated and then can find the solution of Eqn (7).

Appendix B: Expansions in VDS

As discussed in Isotopic mass conservation, the product $\delta^{13}CO_2 \times CO_2$ is conservative. Analogue to CO_2 (Chen *et al*., 2004a), therefore, algorithms for CO_2 mole fraction

of air (CO_2) can be used for carbon isotopic simulation. For the stable/nocturnal module, analogous to Eqns (1b) and (2b) in Chen *et al*. (2004b), we have

$$F_{\delta 13,j} = -K_{c,j}\frac{X_{j+1/2} - X_{j-1/2}}{z_{j+1/2} - z_{j-1/2}} \quad (j = 1, \ldots, 50), \tag{B1}$$

$$\frac{X_{j-1/2,t+\Delta t} - X_{j-1/2,t}}{\Delta t} = -\frac{F_{\delta 13,j} - F_{\delta 13,j-1}}{z_j - z_{j-1}} \quad (j = 1, \ldots, 50), \tag{B2}$$

where X denotes $\delta^{13}CO_2 \times CO_2$ in $\mu mol\,m^{-3}$ ‰); $F_{\delta 13}$ is positive for upward fluxes ($\mu mol\,m^{-2}\,s^{-1}$ ‰); K_c is the eddy exchange coefficient in $m^2\,s^{-1}$ (see Appendix B in Chen *et al*., 2004b); z is the height above the ground in m; Δt is the computing time step (=30 s, in this study); the subscript j denotes the model layer (with a vertical interval of 50 m); while $j+1/2$ or $j-1/2$ denotes the middle levels between the adjacent layers. For the free convection module (analogous to Eqns (5b) and (15) in Chen *et al*., (2004a)), Eqns (B3) and (B4) are used for each layer above the surface layer and in the surface layer, respectively:

$$\frac{\partial X_{j-1/2}}{\partial t} = \beta_{m_{1,j-1/2}}(X_s - X_{j-1/2}) + \beta_{m_{2,j-1/2}}(X_t - X_{j-1/2}), \quad j \geq 2, \tag{B3}$$

$$\frac{\partial X_s}{\partial t} = \left[F_{\delta 13,s} - \beta_{m_1,j-1/2}\sum_{2}^{J_{CBL}}(X_s - X_{j-1/2})\Delta z\right]/(z_1 - d), \tag{B4}$$

where the subscripts s and t represent the values at the lower surface layer and at the top of model domain (the model boundary values, see Model boundary conditions), respectively; d is the displacement height in m (=$0.67h_c$), J_{CBL} is the maximum number of layers in the growing CBL, $J_{CBL} = \text{int}[z_h/\Delta z]$, z_h is the height of CBL (see Appendix B in Chen *et al*., (2004a), $\Delta z = 50$ m; $\beta_{m_{1,j-1/2}}$ and $\beta_{m_{2,j-1/2}}$ denote the fractions of total mass exchange between the model layer j and the lower surface layer per unit time and between the model layer j and the top of the mixed layer per unit time, which are expressed as

$$\beta_{m_{1,j-1/2}} = Q_{h,s}/\rho c_p\left(\sum_{2}^{J_{CBL}}(\theta_s - \theta_{j-1/2})\Delta z\right)^{-1}, \tag{B5a}$$

$$\beta_{m_{2,j-1/2}} = cQ_{h,s}/\rho c_p\left(\sum_{2}^{J_{CBL}}(\theta_s - \theta_{j-1/2})\Delta z\right)^{-1}, \tag{B5b}$$

where θ_s and $\theta_{j-1/2}$ are the virtual potential temperatures in the lower surface layer and in the $j-1/2$ layer, respectively; $Q_{h,s}$ is the sensible heat flux in the surface layer in $W\,m^{-2}$; c is the ratio of the sensible heat flux at the top of CBL $(\overline{\theta' w'})_{z_h}$ to the value in the surface layer $(\overline{\theta' w'})_0$; ρ is the density of air; c_p is the specific heat of air, and $\Delta z = 50$ m. Note that, the CO_2 mole fraction of air for each model layer is also simulated using these similar equations at each time step. Once we gain the values of X and CO_2, the value of $\delta^{13}CO_2$ is the quotient of X and CO_2.